Microchim Acta (2017) 184:649–675
DOI 10.1007/s00604-017-2093-7

REVIEW ARTICLE

Nanomaterial-based electrochemical sensors and optical probes for detection and imaging of peroxynitrite: a review

Alina Vasilescu[1] · **Mihaela Gheorghiu**[1] · **Serban Peteu**[2]

Received: 11 November 2016 / Accepted: 17 January 2017 / Published online: 1 February 2017

Abstract Peroxynitrite (PON for short) is a powerful nitrating, nitrosating and oxidative agent for cellular constituents. In vivo, PON is formed through the diffusion-controlled reaction between superoxide radical ($O_2^{\bullet-}$) and nitric oxide (•NO). This critical review (with 67 refs.) covers the state of the art in nanomaterial-based (a) detection and imaging of PON inside cells and (b) monitoring of cellular events such as cellular oxidative burst by using optical or electrochemical methods. It starts with the formation, fate and pathophysiology of PON in vivo. The next part summarizes nanomaterial based electrochemical microsensors featuring nanofilms and nanostructured electrodes, nanospheres, 3D nanostructures and graphene-supported catalysts. A following chapter covers techniques based on optical nanoprobes, starting with nanomaterials used in optical detection of PON (including quantum dots, carbon dots, fluorescent organic polymer dots, rare earth nanocrystals including upconversion nanoparticles, iron oxide nanoparticles, gold nanoparticles, and fluorophore-modified nanoporous silicon). This is followed by subsections on strategies for optical detection of PON (including color changes, fluorescence quenching, activation and recovery), and on schemes for optimized spatial and temporal resolution, for improving sensitivity, selectivity, and (photo)stability. We then address critical issues related to biocompatibility, pharmacokinetics, give a number of representative practical applications and discuss challenges related to PON detection. The review concludes with a discussion of latest developments and future perspectives.

Keywords Selectivity · Response time · Dynamic assay · Graphene · Short lived species · Ratiometric fluorescence · Theranostic · Biocompatibility

Abbreviations

AG	Aminoguanidine
AuNCs	Gold nanoclusters
AuNPs	Gold nanoparticles
BzSe-Cy	Benzylselenide-tricarbocyanine
CA	Citric acid
CV	Cyclic voltammetry
CDs	Carbon dots
CF-SPN	Semiconductor polymer nanoparticles for combined CRET and FRET
CLIO	Cross-linked iron oxide
CRET	Chemiluminescence resonance energy transfer
DCF	2′,7′-dichlorofluorescein
DL	Detection limit
EPR	Enhanced permeability and retention
FRET	Fluorescence resonance energy transfer.
GCE	Glassy carbon electrode
GSH–$_{TGA}$–CdTe@ ZnS	Core-shell quantum dots with CdTe core capped with TGA and shell of ZnS capped with GSH (GSH–$_{TGA}$–CdTe@ ZnS)
HA	Hyaluronic acid
iNOS	Inducible nitric oxide synthase
IRhB	Isopropylrhodamine B

Alina Vasilescu and Mihaela Gheorghiu have contributed equally to this paper.

✉ Serban Peteu
peteu@msu.edu

[1] International Centre of Biodynamics, 1B Intrarea Portocalelor, 060101 Bucharest, Romania

[2] Department of Chemistry, Michigan State University, 578 S Shaw Lane, East Lansing, MI 48824, USA

IUPAC	International Union of Pure and Applied Chemistry
LPS	Lipopolysaccharide
LRET	Luminescent energy transfer
MacTNP	Macrophage-targeted theranostic nanoparticles
MPS	Mononuclear phagocytic system
Mn-pDPB	Manganese-[poly-2,5-di-(2-thienyl)-1H–pyrrole)-1-(p-benzoic acid)] complex
MTT	3-(4,5-dimethylthiazol-2-yl)-2,5-diphenyltetrazolium bromide) tetrazolium reduction assay
NIR	Near infrared
NSET	Nanometal-surface energy transfer
PA	Photoacoustic
PEDOT	Polyethylene-dioxythiophene
PEI	Polyethyleneimine
PFODBT	Poly[2,7-(9,9′-dioctylfluorene)-*alt*-4,7-bis(thiophen-2-yl)benzo-2,1,3-thiadiazole]
PMA	Phorbol 12-myristate 13-acetate
PN-CDs	Phosphorus and nitrogen doped carbon dots
PON	Peroxynitrite
PS-*g*-PEG-Gal	Galactosylated graft copolymer of poly(styrene) and poly (ethylene glycol)
PVP	Polyvinylpyridine
RES	Reticuloendothelial system
rGo	(Reduced) graphene oxide
RNS	Reactive nitrogen species
RONS	Reactive oxygen and nitrogen species
ROS	Reactive oxygen species
RT	response time
SPNs	semiconductor polymer nanoparticles
TEMPO	2,2,6,6-tetramethyl-1-piperidinyloxy
TGA	Thioglycolic acid
TPCP Mn	Mn (III)- paracyclophenylporphyrin
Trp-CD	Tryptophan carbon dots
UCL	Upconversion luminescence
UCNP	Upconversion nanoparticles
WE	Working electrode

The formation, fate and pathophysiology of peroxynitrite in vivo

Peroxynitrite ($ONOO^-$ or PON for short) was established in the last decade as a powerful nitrating, nitrosating and oxidative agent for cellular constituents a mediator of superoxide radical and nitric oxide-dependent oxidative and cytotoxic processes. The main reactive oxygen species (ROS) and reactive nitrogen species (RNS) [1] are illustrated in Scheme 1.

Starting in the 1990s, the seminal publications by J. S. Beckman, H. Ischiropoulos, R. Radi and others [2, 3, 4] suggested the biological formation of peroxynitrite by the near diffusion-controlled reaction between nitric oxide and superoxide radicals implicated in oxidative injury and inflammation [2, 3, 5–8]. Ever since, solid clinical evidence shows that endogenously generated PON is correlated with acute cytotoxicity and thus incriminated in various pathologies and diseases [2, 3, 4]. The PON pathogenic effects have been aptly reviewed [2, 3, 4, 9]. Thus perhaps rightfully, PON anion is hailed as the "ugly side" of nitric oxide, that in turn acts as a "good" molecule, whose low level production is important in protecting organs, such as the liver, from ischemic damage. The trio (•NO; $O_2^{\bullet-}$; $ONOO^-$) was notably dubbed [2] as "the Good, the Bad and the Ugly". Peroxynitrite affects mitochondrial function, triggers cell death via oxidation and nitration reactions, acts as an endogenous toxicant. Yet it is also a cytotoxic effector against invading pathogens. The biological chemistry of peroxynitrite that has a life time of only about one second at physiological pH [10] is modulated by endogenous antioxidant mechanisms. PON is also neutralized by synthetic compounds with peroxynitrite-scavenging capacity. [2, 10]. As such, PON assessment although a matter of intense scrutiny is still characterized by important challenges: achieve high specificity, intracellular cell access, reproducible and quantifiable signals, improved time and spatial resolution. Addressing these challenges, nanomaterial-based approaches have been used in conjunction with electrochemical and optical methods for the detection of PON (a), imaging of PON inside cells (b) and monitoring cellular events such as cellular oxidative burst (c). Although there are not many reports so far, the nanomaterials investigated covered a wide range, from

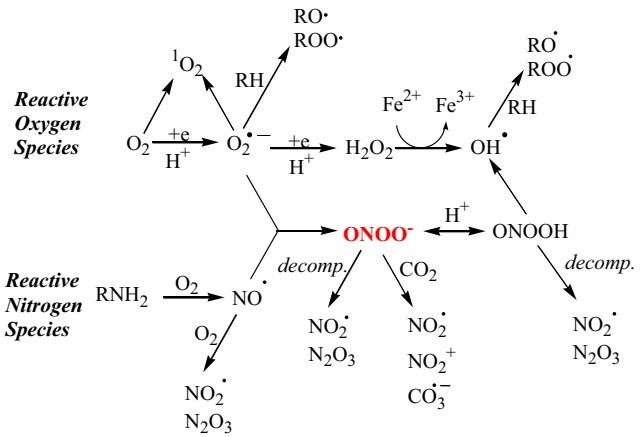

Scheme 1 The principal ROS and RNS species derived from the biological conversion of oxygen into superoxide ion and nitric oxide, redrawn from [1]

quantum dots and nanoparticles to graphene-based materials and polymeric nanoprobes/nanostructured films. The specific advantages brought by the use of nanomaterials in applications centered on peroxynitrite are critically presented in this review. Some representative examples and the related challenges are discussed in more detail.

Nanoscale properties and interaction of nanomaterials with PON

The unique properties of materials at nanoscale provide several advantages in nanomaterial-based electrochemical and optical probes for PON, similarly to the detection of other analytes. In electrochemical probes for example, high surface-to-volume ratio, good electrical conductivity, biocompatibility, catalytic ability and easiness of functionalization with conductive polymers, metallic nanoparticles (NPs) or catalysts for PON oxidation such as manganese and porphyrin complexes provide numerous ways to improve sensor performance. Nanostructured electrodes provide a large electroactive area promoting the surface adsorption and fast sensor response for PON. Nanosized electrodes allow detecting of reactive oxygen species (ROS) in the vicinity of single cells or inside macrophages, where they can be inserted without causing irreparable damage to the cell membrane. Nanoelectrochemical sensors display good sensitivity and temporal resolution for monitoring oxidative bursts.

Nanomaterials can assist indirectly with PON detection by preventing unwanted reactions at electrode surface, e.g. the unwanted self-polymerisation of hemin is prevented in graphene-supported hemin [11]. Nanomaterial-based electrodes can be furthermore coated with permselective membranes to further improve selectivity for PON. Electrode modification with nanomaterials is achieved by various strategies including physical adsorption (e.g reduced graphene oxide-hemin film [11] deposited on glassy carbon electrode), electrodeposition (Pt on C microfiber [12]) and electropolymerization with redox polymers [12–15].

In electrochemical probes, PON interacts with catalytic nanofilms or hybrid nanomaterials deposited on electrode surface and the result is increased sensitivity and lower overpotential for PON detection compared to the bare electrodes.

With regards to optical detection and bioimaging in the intracellular environment, there are definite advantages associated with use of nanomaterial-based transducers compared to dyes and fluorescent proteins, as shown for relevant biological analytes including ROS [16–18]. Nanoprobes confer improved spatial resolution and better contrast, allowing high quality imaging in vivo and in cell cultures. Nanoprobes have higher brightness and photostability compared to molecular probes [19], are or can be made inert to non-specific binding by cellular proteins and display low cytotoxicity. NPs can be internalized by cells depending on their charge and size. Increased uptake and retention of nano sized objects by tumor cells as compared to healthy ones has been reported. This effect called “Enhanced Permeability and Retention” (EPR) is due to pores (named “fenestrations”) in the angiogenic blood vessels supplying the tumors but was also observed in inflamed tissues [20]. Among practical aspects one should note the simpler handling compared to fluorescent proteins and the commercial availability of many types of NPs [19].

Some nanoparticles, such as Au nanoclusters (Au NCs), Au NPs, carbon dots (C-dots) and quantum dots (QDs), present inherent optical properties, which eliminate the need for labelling with a reporter probe. Spatial confinement of conduction electrons in AuNPs and Au NCs (smaller than 3 nm, [21]) generates size-dependent surface plasmon resonance adsorption in AuNPs and strong photoluminescence of AuNCs [22]. QDs are semiconductor nanoparticles of only a few nanometers, composed of elements from the periodic groups II–VI (CdS, CdSe, CdTe) or III–V (e.g. GaAs). Due to their extremely small size, the confinement of electron-hole pairs in QDs gives rise to interesting optical properties such as bright fluorescence, which can be tuned by changing the size, composition and shape of QDs. C-dots contain mainly carbon, oxygen and hydrogen, their fluorescence emission is in the visible and near-infrared (NIR) range and certain types of C-dots exhibit upconverted photoluminescence. Fluorescence emission spectra of the C-dots are determined by several factors, including excitation wavelength, particle size, shape, composition and internal structure [20].

Nanomaterials such as AuNPs, semiconductor polymer nanoparticles (SPNs) and upconversion nanoparticles (UCNP) display several energy transfer mechanisms at nanoscale, such as nanometal surface energy transfer (NSET), fluorescence resonance energy transfer (FRET), luminescence energy transfer (LRET), or chemiluminescence resonance energy transfer (CRET) which can be exploited for sensitive imaging of PON. These properties depend on the size of NPs and the distance between the acceptor and the donor fluorophore. Moreover, there are a myriad of design possibilities, from simple nanoparticles of various sizes to complex nanostructures (core-shell, nanoclusters etc). Particularly appealing are those with dual functionality, e.g. in theranostics and those capable of self-referencing, which include two different fluorophores (e.g. one specific for the target analyte and a second dye acting as internal reference). NPs can be coated and functionalized by various strategies and can act as cargo and be loaded with a vast variety of molecules. The high surface-to-volume ratio of NPs and convenient manipulation of surface chemistry allows efficient immobilization of reporter probes while ensuring biocompatibility, inertness and enhanced targeting of cells and subcellular entities.

In optical nanoprobes, PON interacts with nanomaterials in several ways. For example, PON's oxidative action increases the fluorescence of nanomaterial-attached dye without breaking the bond between the fluorescent reporter and the supporting nanomaterial [23]. Interestingly, in the presence of reducing agents such as glutathione, the oxidation of DCFH (reduced 2′, 7-dichlorofluorescein) to DCF (2′, 7-dichlorofluorescein) can be reversed as shown for a proof-of-concept nanoreactor allowing monitoring PON-glutathione redox reaction by fluorescence switching in real time [23].

PON can quench the intrinsic fluorescence of nanomaterials such as Au nanoclusters or QDs by oxidizing Au nanoclusters to Au (I) [24] and by breaking the QD-thiolate bond [25], respectively. Irreversible cleavage by PON of bonds within nanomaterial-attached dyes leads to abolishment of energy transfer mechanisms behind the quenched fluorescence of such nanoprobes [26, 27] and release of fluorescent reporters [28] or restauration of fluorescence [27, 29].

One of the major effects of PON is the damage of DNA. When associated with DNA adsorption on Au NPs, it causes particle aggregation by abolishing the electrostatic interactions warranting the stability of AuNPs, well covered by intact DNA [24]. Nanoparticle aggregation is simply detected by colorimetry.

The optical and electrochemical properties, as well as the behavior and stability in real samples such as cells or tissues are determined by the basic characteristics of nanoparticles related to the material nature, surface chemistry, surface charge and size. While these correlations were discussed in several reviews [11, 16–20, 30, 31], examples on the role of these characteristics on the sensitivity and selectivity of PON detection will be given further along.

Electrochemical methods with nano-material based microsensors

PON electrochemical microsensors feature nano-films, nanospheres, 3D nano-structures, or nano-channels and the field has witnessed significant advancements in terms of the quantification mechanism and response performance (detection limit, sensitivity and measuring range). Table 1 outlines several significant contributions. The specific concepts, advantages, drawbacks and challenges of the various methods are briefly reviewed below.

The group of Amatore has developed several innovative methods [2, 36, 37] supported by both theoretical and experimental models, including nano-sensors [2]. Among these, one technique involved the concurrent quantification of •NO, $O_2^{\bullet-}$ and $ONOO^-$ in the vicinity of a single cell [10, 38] using disk type, flat nanoelectrodes. The amperometric studies performed on fibroblast cells at different oxidative potentials have shown a complex response that apparently incorporated multiple electroactive species as oxidative waves, successively confirmed by in vitro experiments. Figure 1 illustrates the species H_2O_2, $ONOO^-$, •NO, NO_2^- being directly oxidized by Pt-C-microfiber electrodes (Pt-C μFEs) at their distinct potentials vs. a standard saturated calomel electrode (SSCE).

The integration of the reconstructed fluxes of the RNOS allowed the calculation of an average total amount of each species, detected as shown in Fig. 1 [2]. This intriguing assay procedure allowed the exploration of a carefully controlled biological environment; however its merits still remain to be fully appreciated for unknown, complex in vivo configurations.

Nanometer-size electrodes are needed for in vivo electrochemical measurements as they are inserted within living cells without causing irreparable damage to the cell membrane. Also, it is essential to ensure that the cell membrane formed a tight seal around the nanoelectrode shaft, to eliminate the possibility that the response monitored inside the cell result from traces of species released outside the same that leaked into the cell. Amatore's group prepared disk-type, flat nanoelectrodes by subsequently pulling a 25-μm-diameter annealed Pt wires into borosilicate glass capillaries, followed by micropolishing. Nanoelectrodes were etched with an alternating current, to create a e cca. 40 nm nano-cavity [32]. The nanocavity was finally filled with Pt black by electrodeposition. Compared to the simple Pt polished nanoelectrodes, the etched nanoelectrodes with electrodeposited Pt black presented similar voltammograms for the ROS/RONS produced in macrophages, namely PON, H_2O_2, NO and NO_2^- but higher sensitivity, and better stability of the electrodes against passivation due to ROS/RONS [32]. Thus, the combination between nano size of the electrode and a nanodeposit of catalytically active Pt black represents a successful strategy for in vivo detection of ROS/RNS and illustrates some of the advantages of nanomaterials and nano structuring.

Also notable are several synthetic manganese nanocomplexes employed as components in $ONOO^-$ sensitive electroactive films on electrodes. For instance, Koh and colleagues [12] synthesized a manganese–polymer nanocomplex film with the polydithienyl-pyrrole-benzoic acid (pDPB) by electrodeposition onto a Platinum (Pt) μEs.

The cloud density of the atoms in PON is as follows:

−0.288−0.130−0.122−0.458
O–N–O–O*

The O* atom has maximum cloud density thus it can provide the low-pair electrons to the center of the Mn atom (cloud density of 0.252) of the Mn nanocomplex, formed as an axial coordinating compound. The Fe based nanocatalysts undergo similar molecular interactions. The conductive polymer pDPB film was prepared reproducibly down to nm dimensions

Table 1 Approaches for the Electrochemical detection of peroxynitrite using nanomaterials

Nanomaterial characteristics	Electrode details	Working principle	Analytical performances	Real sample/selectivity	Reference
40 nm cavity in Pt nanoelectrode with electrodeposited Pt black.	WE polarized at +0.85 V vs. Ag/AgCl	Electrocatalytic oxidation of PON	RT = 50 ms DL = 10 fM	In vivo detection inside murine macrophages of total ROS/RONS (PON, NO_2^-, H_2O_2 and NO)	[32]
Pt microelectrode with a Mn-pDPB film deposited with Au nanoparticles. A PEI membrane applied to confer selectivity	WE polarized +0.2 V vs. Ag/AgCl	Reduction of PON	RT = 15 s DL = 1.9 nM	PON detection in rat plasma. Selective versus bilirubin, ascorbic acid, serotonin, dopamine	[13]
rGO-hemin film on GCE	WE polarized +1.1 V vs. Ag/AgCl	Electrocatalytic oxidation of PON	RT = 20 s DL = 5 nM	N/A	[11]
Nanostructured PEDOT-hemin film	WE polarized at +1.25 V vs. Ag/AgCl	Electrocatalytic oxidation of PON	RT = 5 s DL = 200 nM	Selective versus NO_2^-, NO_3^-	[14, 33]
		Electrocatalytic oxidation of PON	RT = 3.5 s DL = 10 nM	N/A; selective versus norepinephrine, serotonin, uric acid	[34]
rGO/CoPc-COOH on GCE electrode	WE polarized at +1.1 V vs. Ag/AgCl	Electrocatalytic oxidation of PON	DL:1.7 nM	N/A/ selective versus NO_2^-, NO_3^-, H_2O_2, dopamine, glucose	[35]
C fiber tip sharpened at 200 nm. Covered with nanofilm of TPCP Mn and PVP	WE polarized at −0.3 V vs. Ag/AgCl	PON reduction	RT = 1 ms DL = 1 nM	Detection at surface of endothelial cells	[15]

PON Peroxynitrite; *RNOS* Reactive nitro oxidized species; *WE* Working electrode; *RT* Response time; *DL* Detection limit; *Mn-pDPB* Manganese-[poly-2,5-di-(2-thienyl)-1H–pyrrole)-1-(p-benzoic acid)] complex; *rGO* Reduced graphene oxide; *PEI* Polyethyleneimine; *GCE* Glassy carbon electrode; *PEDOT* Polyethylenedioxythiophene; *PVP* Polyvinylpyridine; *TPCP* Mn = Mn (III)- [2] paracyclophenylporphyrin

ensuring a stable and rapid response time. This (Mn-pDPB) film was decorated with electrodeposited Au nanoparticles that reportedly enhanced the PON reduction, according to the reaction scheme from Fig. 2a and calibration graph from Fig. 2 b. Moreover, an increase in selectivity was reported by using an outer layer of polyethyleneimine (PEI). The interferents tested included several electroactive species and PON decomposition molecules [12]. The selectivity was reported as satisfactory, allowing these Mn-pDPB-PEI μEs to be employed for the PON determination in vitro on glioma tumor cells. To further validate this work, it would be useful to repeat the same experiments with the "genuine" synthetic PON freshly prepared.

The group of Malinski [14, 39, 40] used a manganese(III) paracyclophenyl-porphyrin (MnPCP) nano-thin film electrodeposited on carbon microfiber nanoelectrodes (CFnE) for PON detection in the presence of •NO and $O_2^{\bullet-}$. The chronoamperometry was conducted with the three working electrodes poised at different potentials, namely 0.67 V for •NO, 0.35 V for $O_2^{\bullet-}$ and −0.35 V for $ONOO^-$. The tip of the carbon fiber was gradually burned with a propane microburner to reduce its diameter down to 200–300 nm. Subsequently, this tip was modified with a thin MnPCP film. The overall nano-dimensions of the measuring tip allowed a very fast response time that followed the peroxynitrite released in real time. Detection was based on the reduction of

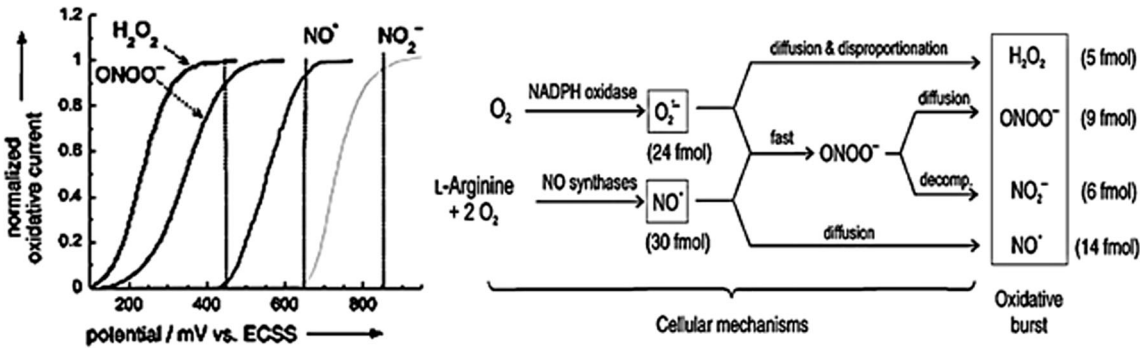

Fig. 1 The species H_2O_2, $ONOO^-$, NO, NO_2^- being directly oxidized at their distinct potentials and their reconstructed fluxes. Reproduced from [2] with permission from Wiley

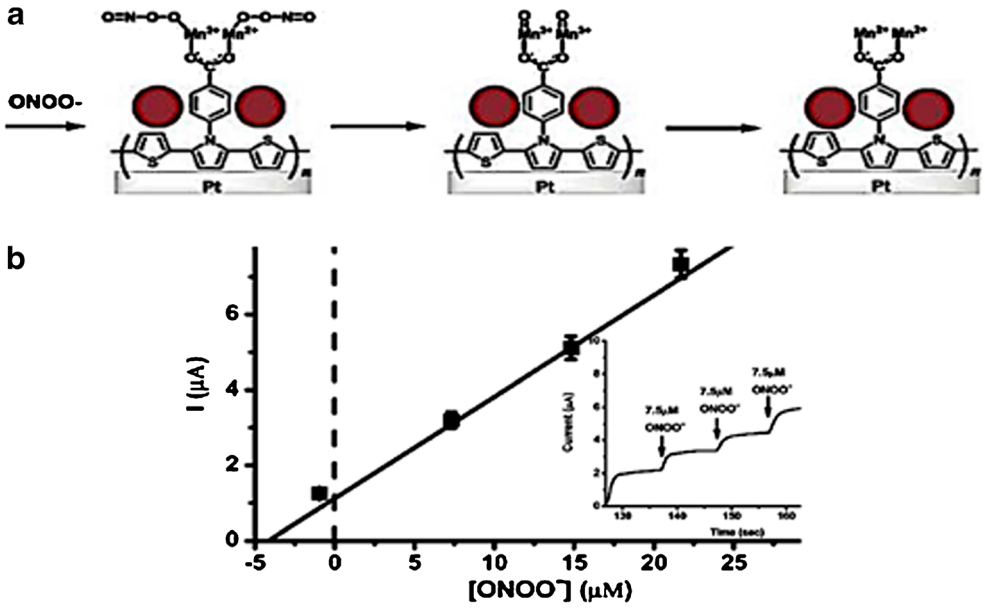

Fig. 2 The PON-sensitive manganese nano-complexes (**a**) and the resulting calibration graph (**b**). Reproduced from [12] with permission from the American Chemical Society

$ONOO^-$. The concentration ratio [•NO] / [$ONOO^-$] was reported as a potentially useful marker to diagnose cardiovascular disease [14]. The same group quantified PON after release upon stimulation by a beta-blocker medication, Nebivolol [39] as illustrated in Fig. 3 below.

Bayachou and Peteu [13, 33] used a nano-thin film of the electroactive, intrinsically conductive polymer polyethylenedioxythiophene (PEDOT) together with hemin (Fig. 4) electro-assembled on carbon fiber microelectrodes for the detection of $ONOO^-$. The response to PON of the hemin film was compared, with and without PEDOT, with cyclic voltammetry and amperometry. When PEDOT was present the sensitivity was strongly enhanced, as compared to just the hemin film or the PEDOT film. Significantly, the typical "nano-cauliflower" tortuous and porous matrix of the hemin-PEDOT hybrid seemed to provide a very high specific area/volume, as seen in SEM from Fig. 5a [13]. This testing has suggested that synergy occurs between the PEDOT and the hemin macrocycle molecules; this hypothesis was supported by a decrease of the oxidation potential for the nano-hybrid material, as compared with the responses from either of the two components employed separately (Fig. 5). The hemin-PEDOT film was revealed as a fractal 3-dimensional matrix with an inherent peak-and-valley nano-structured surface and features in the 100–300 nm range. This implies that the PON analyte molecule must travel a much longer path though the twisted pores from the outer surface to the inner catalytic sites within the hemin-PEDOT film. Consequently, this results in a larger contact surface between the catalyst and the analyte, thus an increase in the ratio current-to-analyte concentration leading to a higher sensitivity. Herein, the electroactive PEDOT allows a precise control upon its electrodeposition as a nano-film with high conductivity mediating a fast electron transfer.

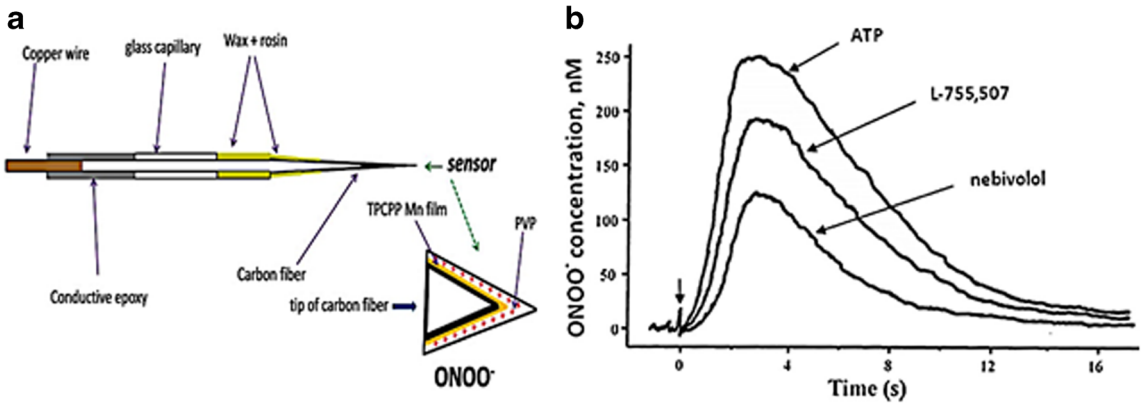

Fig. 3 The PON-sensitive C fiber microelectrodes (**a**) and the PON quantified after release, upon stimulation by a beta-blocker (**b**). Reproduced from [38] with permission from Springer and from [37] with permission from BioMed Central Ltd., under the terms of the Creative Commons Attribution License (http://creativecommons.org/licenses/by/2.0)

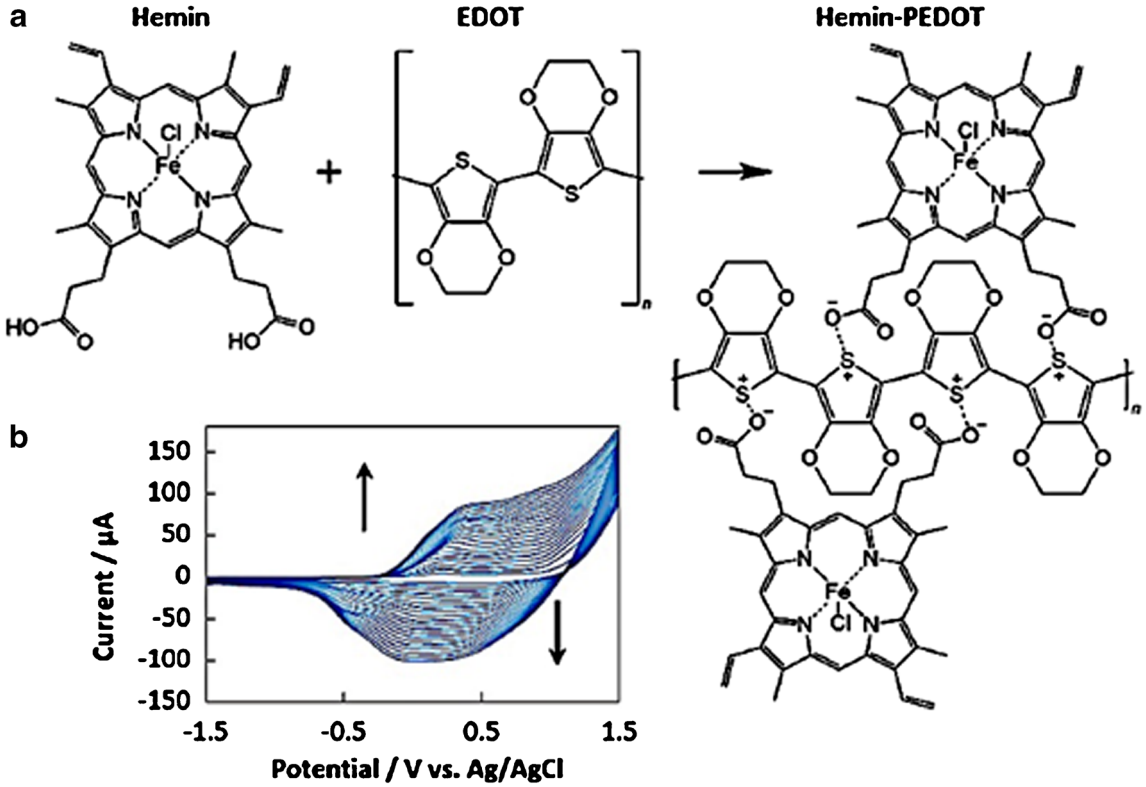

Fig. 4 The complex hemin-PEDOT (**a**) and its polymerization (**b**). Reproduced from [13] with permission from the Royal Society of Chemistry

Szunerits, Peteu and colleagues built on their earlier published methods [11, 41] for preparing a hemin-functionalized reduced graphene oxide to prepare PON-sensitive electrodes [11]. A graphene oxide aqueous solution was mixed with hemin with subsequent sonication for several hours, resulting in hemin-rGO (Fig. 6), that was next drop-casted onto GCEs. The hemin-rGO modified GCE has shown an oxidative wave at 1.17 V that was ascribed to the electrochemical oxidation of

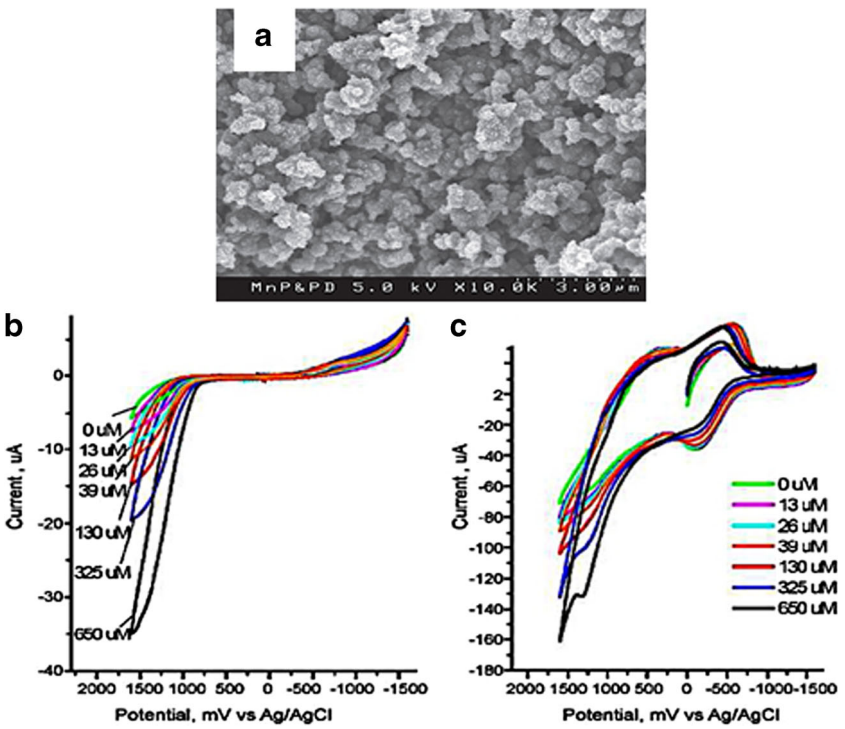

Fig. 5 The response of the nanostructured PEDOT-hemin (**a**) to PON of the hemin film was compared, with and without PEDOT (**b, c**). Reproduced from [13] with permission from Elsevier

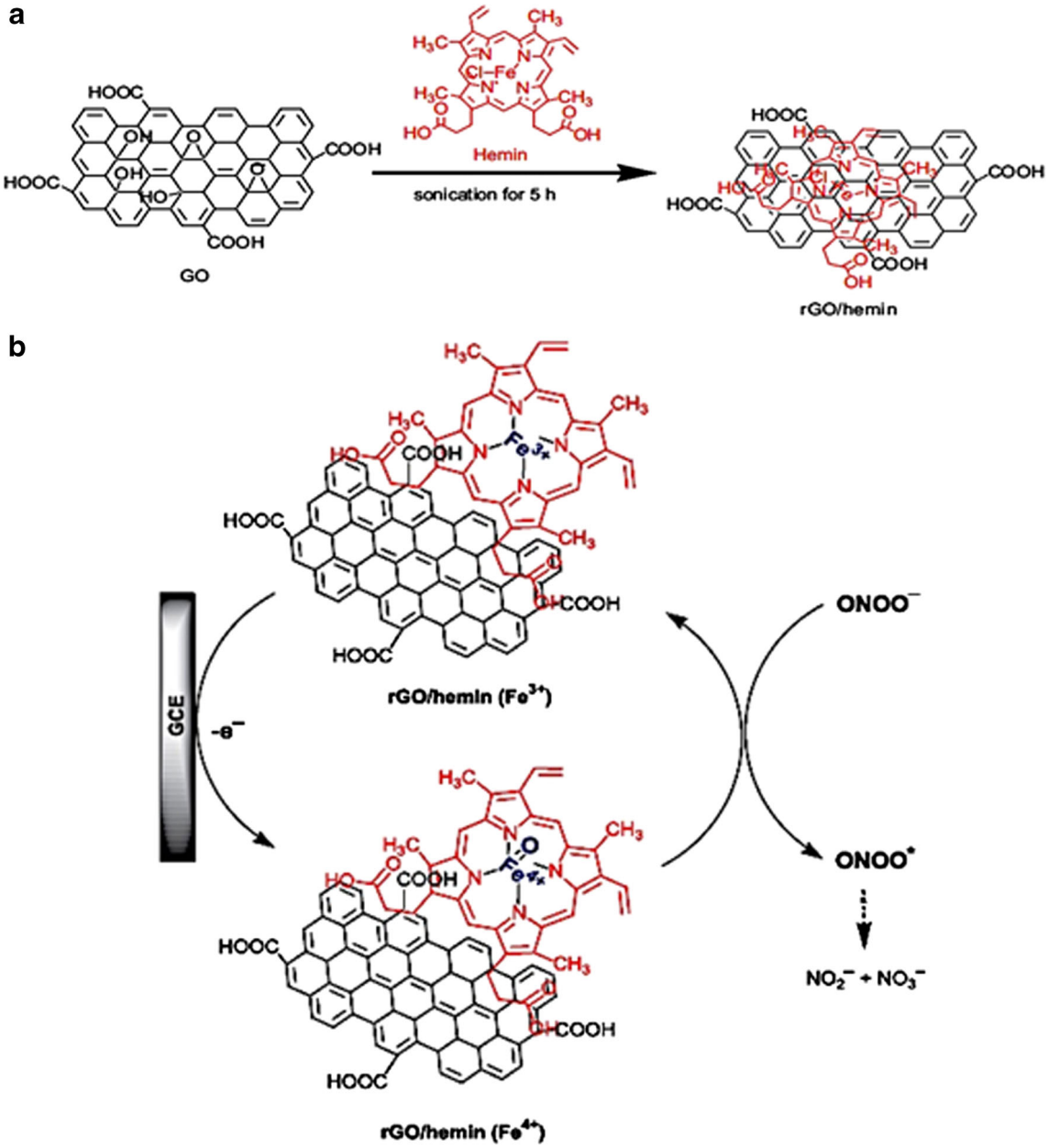

Fig. 6 The preparation of the hemin-reduced graphene oxide (**a**) and its response to PON (**b**). Reproduced from. [11] with permission from the Royal Society of Chemistry

hemin on the rGO platform. In the presence of $ONOO^-$ from SIN-1, an electrocatalytic oxidation mediated by hemin centers seems to occur, as illustrated by the reaction mechanism in Fig. 6.

The Fe^{3+} center of hemin in the rGO–hemin film was oxidized electrochemically at the electrode interface to a high valent iron form such as [Fe^{4+} = O] iron oxo intermediate. In the PON presence, this intermediate is reduced back to Fe^{3+} for further turnovers [11]. The resulting current scaled linearly with the PON concentration, and a detection limit of 5 ± 0.5 nM was recorded in PBS with a sensitivity of 7.5 nA nM^{-1} [11]. The reasons for this apparent increased sensitivity brought by graphene needs to be elucidated. Firstly, graphene provides a two-dimensional support with large open accessible surface with high area per volume ratio, where the catalyst-PON interaction seems to be enhanced, which seems beneficial for the surface-driven electrocatalytic activity. Secondly, the graphene-supported hemin appears to prevent hemin molecules from self-polymerization and thus increase the available iron-hemin catalytic active sites. Thirdly, the amount of hemin present on the electrodes seems to be important; the amount incorporated into the new rGO/hemin matrix is 2.5 times larger than that on rGO that is post-modified with hemin. Ongoing research seeks a better understanding of the

catalytic mechanisms of graphene supported hemin for PON oxidation and to develop highly sensitive sensor platforms [32].

Meanwhile, Peteu and Swain [34] reported the modification of a Boron doped diamond (BDD) microelectrode with an electropolymerized PEDOT-hemin film. Again, the presence of PEDOT was correlated with a sensitivity increase towards PON, for reasons already mentioned herein. The nanostructured modified polymer layer was characterized by Raman spectroscopy and scanning electron microscopy (SEM). The measured detection limit for PON was 10 ± 0.5 nM (S/*N* = 3), the sensitivity was 4.5 ± 0.5 nA nM^{-1} and the response time was 3.5 ± 1 s. A polyethyleneimine (PEI) layer was applied on the tip to make the sensor selective to PON in the presence of norepinephrine, serotonin and uric acid [34] as seen in Fig. 7.

Optical techniques with nano-probes for assessment of PON

Overview

Electrochemical and optical sensors are complementary tools for assessing PON and ROS in general. Fast electrochemical sensors allow temporal resolution and are very useful in vitro for gathering quantitative data on the PON fluxes, at single cell level, and probing the underlying mechanisms of various physiological process. However, their use in vivo is complicated, due, among others, to issues related to implanting the sensors. In contrast, many of the optical probes are considered minimally invasive, have low cytotoxicity and favorable pharmacokinetics (good blood circulation and appropriate clearance from the body), and can be used with either passive or targeted delivery. Optical probes allow large area imaging of PON and ROS (even imaging of a whole small animal) getting representative pictures of the extent of ROS generation and the localized effect of different drugs. They also allow mapping intracellular ROS. An important advantage of nanomaterial-based optical probes is their possibility to be used in theranostics as it will be discussed further below.

The last years witnessed an increased research effort towards developing better probes for detection and imaging of PON and ROS in general [16–18], prompted by the need to elucidate the role played by these reactive species in key biological processes related to the onset of various diseases (Table 1). Compared to other analytes, optical detection of PON/ROS imposes the additional requirements of speed, reversibility and high sensitivity of response, to be able to detect short lived radical species and their fluxes at relevant physiological levels [16]. Moreover, the specificity of detection is paramount to elucidate the particular role of a certain radical species, such as PON, in physiological events. Optical methods reporting on PON detection and imaging use traditionally: (i) ROS-sensitive small fluorescent probes, (ii) genetically engineered proteins and (iii) nanostructures, taking advantage of the unique physico-chemical and optical properties of materials at the nano scale and their interaction with fluorescent reporters, as discussed in section 2.

Nanomaterials used in optical detection of PON

Not surprisingly, the emergence of nanomaterials has brought a wealth of design possibilities and functionalization strategies that are exploited in order to reach optimum characteristics for detection. The main characteristics of various types of nanoparticles, their coatings and approaches for surface functionalization in relation to their applications in bioimaging have been reviewed elsewhere [16–20, 30]. Several relevant examples of nanomaterial-based methods applied for PON detection and imaging in biological samples are presented in Table 2, relying on fluorescence, chemiluminescence and colorimetric detection.

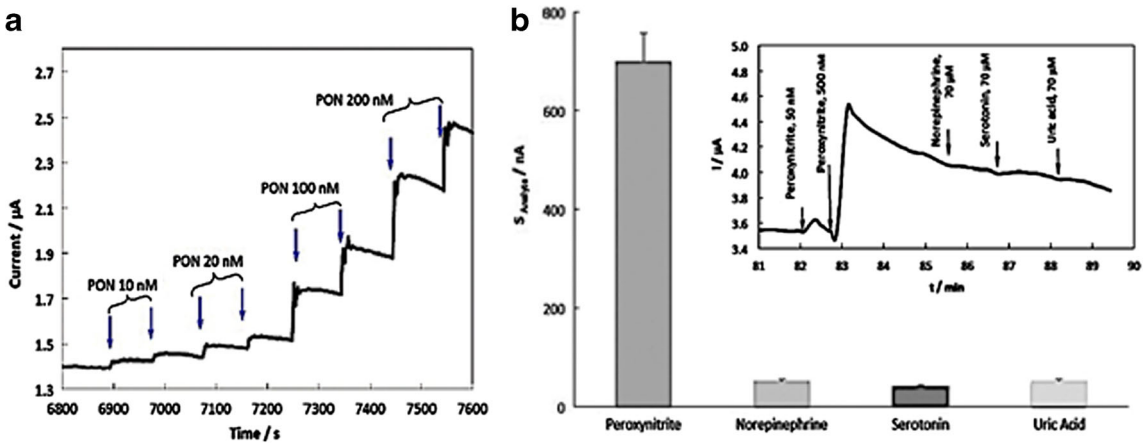

Fig. 7 The detection limit (**a**) and selectivity (**b**) of the PON-sensitive BDD microelectrode. Reproduced from [31] with permission from the Royal Society of Chemistry

Table 2 Approaches for the optical detection and imaging of peroxynitrite using nanomaterials

Nanomaterial characteristics	Probe details	Principle	Analytical performances	Sample	Reference
Thiol-capped CdTe and CdTe@ZnS quantum dots; 2.6 nm–3.3 nm, Φ_F = 0.39–0.72	λ_{exc}: 400 nm, λ_{emm}: 557 nm (MPA–TGA–CdTe@ZnSQDs) (a) 600 nm (GSH–TGA–CdTe@ZnS,) (b); 566 nm (MPA–CdTe) (c)	Fluorescence quenching by PON	DL: 12.6 nM (a;17.7 nM (b);72.4 nM (c) Best selectivity for (b) for H2O2, O^{2-}, OH^-, NO, NO_2^-, NO_3^-, t-butyl hydroperoxide (TBHP), at pH 9.4.	Chemically synthesized PON in phosphate buffer pH 9.4 and pH 12	[26]
Trp-CD 12–29 nm, with spherical or irregular shape	λ_{exc} = 370 nm/$\lambda_{emm=}$ 457 nm and $\lambda_{exc=}$270 nm/λ_{emm} = 457 nm.	Fluorescence quenching;	DL: 1.5 μM; LR: 5–25 μM; H_2O_2, O_2^-, NO not interfering	Fortified serum	[42]
Phosphorus and nitrogen doped carbon dots (PN-CDs), 1.8 nm.	λ_{exc} = 340 nm, λ_{emm}:406 nm	Fluorescence quenching by ROS/RNS	DL: 0.38 μM (ONOO- LR: 1–60 μM (PON); Stable at pH 4–13 and various ionic strength; Sensitive to ClO^- , $ONOO^-$ $^1O_2$,·OH, NO, insensitive to H_2O_2, O_2^- at 300 μM.	LPS-stimulated RAW264.7 macrophage cells	[43]
Fluorescent carbon dots prepared from citric acid and ethylenediamine; under 10 nm, (quasi)spherical shape	λ_{exc} = 380 nm/ λ_{emm} = 496 nm	Fluorescence quenching	LR: 5–100.0 μM (PON) DL: 2.7 μM Sensitivity at pH 7: PON > OH > NO, H_2O_2, $O_2^{\cdot-}$, NO_2^- and NO_3^-. Selective for PON at pH 10.	Fortified serum. Recovery of 124–129% for 10, 25 and 50 μM PON	[44]
CDs synthesized with citric acid and urea; (quasi)spherical shape, 2.3–8.1 nm	λ_{exc} = 400 nm/ λ_{emm} = 522 nm)	Fluorescence quenching by ClO^- and $ONOO^-$.	Non-selective at pH 7. At pH 9, among various ROS, highest sensitivity was for PON but Fe^{2+} and Fe^{3+} interfere.	Fortified serum. At pH 9, recoveries of 65.1–91.0% for 10, 25 and 50 μM PON	[45]
Polymeric micelle, coated with cell-penetrating peptide; 54.7 nm in solution	λ_{exc} = 635 nm/ λ_{emm} = 810 nm) (BzSe-Cy (indicator dye) λ_{exc} = 532 nm, λ_{emm} = 575 nm (IRhB (reference dye)	Fluorescence quenching of BzSe-Cy by PON.	LR: 0–5 μM for PON. DL: 50 nM. Selective for PON	Live macrophages (RAW 264.7), normal human liver cells (HL-7702) and HepG2 human hepatoma cells	[46]
SPNs of PFODBT/ PS-*g*-PEG-G with encapsulated chemilumines-cence energy donor CPPO, 50 nm, spheri-cal.	detection of H_2O_2 without external light excitation via CRET. λ_{exc} = 580 nm. FRET from the matrix polymer PFODBT (λ_{emm} = 680 nm) to sensing dye IR775S (λ_{emm} = 820 nm). λ_{exc} = 580 nm.	FRET-CRET; chemiluminescence for detection of H_2O_2, and fluorescence for detection of $ONOO^-$ and (^-OCl). (I680/I820).	DL:10 nM for $ONOO^-$ and ClO^- by FRET, DL:5 nM H_2O_2 by CRET. Much higher sensitivity for $ONOO^-$ and ClO^- compared to OH, NO, $^1O_2$, $O_2^{\cdot-}$, H_2O_2.	Real-time in vivo imaging of drug-induced ROS and RNS in mice liver.	[47]
SPN, 78 nm; RONS-inert SPN core (energy donor) covered by RONS-sensitive fluorophore molecules (energy acceptors)	λ_{exc} = 405 nm, λ_{emm} = 678 nm (SPN, FRET donor) and λ_{emm} = 820 nm (IR775COOH FRET acceptor)	Increase in I_{678}/I_{818} nm. upon PON action by abolishing FRET	DL: 10 nM for $ONOO^-$, ClO^- and $^{\bullet}OH$, LR: up to 0.4 μM (for $ONOO^-$ and ClO^- ; LR: up to 0.5 μM for $^{\bullet}OH$; Sensitive to $ONOO^-$, ClO^- and $^{\bullet}OH$, less sensitive to $^1O_2$ $O_2^{\bullet-}$, and NO, not sensitive to H_2O_2.	Detection of ROS at inflammation site in mice;	[27]
Yb/Er co-doped NaYF4 UCNP, functionalized with hyaluronic acid and rhodamine B, 50 nm.	λ_{exc} = 980 nm, λ_{emm} = 540 nm (Rhodamine B).	Enhanced UCL_{540}/ UCL_{654}) due to inhibition of LRET from UCNPs to the conjugated rhodamine B.	DL: 0.06 μM (PON) DL: 0.03 μM ($^{\cdot}OH$), DL: 0.02 μM (ClO^-) DL: 0.1 mM for $O_2^{\cdot-}$	RAW264.7 macrophage cells treated with LPS and PMA, in vivo imaging of arthritic joints in healthy and arthritic mice;	[48]

Table 2 (continued)

Nanomaterial characteristics	Probe details	Principle	Analytical performances	Sample	Reference
				−arthritic mice treated with methotrexate	
MacTNPs self-assembled from HA-Ce6 conjugates; hydrodynamic size of 103.1 ± 38.4 nm; nonfluorescent, nontoxic in native state	λ_{exc} = 400 nm/ λ_{emm} = 660 nm (Ce6).	Fluorescence recovery of Ce6 by ROS via de-quenching upon degrading MacTNP	Much higher sensitivity for PON compared to other ROS such as $O_2^{\cdot-}$, .OH, H_2O_2, ClO− LR: up to 40 μM	Imaging and photodyna-mic therapy of activated macrophages Raw 264.7 cells;	[30]
Alexa Fluor 488 labeled CLIO NPs, coated with ~400 ROS activatable oxazine groups per NP, hydrodynamic diameter 41 nm	oxazine: λ_{exc} = 650 nm/λ_{emm} = 710 nm. Alexa Fluor 488: λ_{exc} = 480 / λ_{emm} = 535 nm	Fluorescence restoration of oxazine upon release of free oxazine by oxidative action of HOCl or PON.	Sensitive to HOCl or PON but stable toward •OH, H_2O_2 and $O_2^{\cdot-}$, NO/O_2, H_2O_2 and ROO•	In vivo monitoring in mouse CD11b-enriched leukocytes; imaging of areas in mouse hearts after myocardial infarction.	[29]
Dual-Emission Fluorescent Nanocomplex of Gold-Cluster- Decorated Silica Particles	λ_{exc} = 405 nm 2Probes: λ_{emm} = 435 nm, (CF 405S succinimidyl ester encapsulated in silica particles, internal reference) and: λ_{emm} = 565 nm, (AuNCs, ROS-sensitive)	Fluorescence quenching (increase of $I_{435}/I_{565)}$	DL: 0.03 μM (•OH), DL: 0.2 μM ($ONOO^-$) DL: 0.5 μM (ClO^-) LR: up to 90 μM ($ONOO^-$)	Live HeLa cells treated with ROS; HL-60 cells, RAW 264.7 cells	[25]
16 nm AuNPs modified with 140 ± 6 fluorescein labeled hyaluronic acid per AuNP ;	λ_{exc} = 488 nm, λ_{emm} = 521 nm	Fluorescence recovery (signal originally quenched due to NSET between Au NPs nanoprobes and fluorescein)	DL: 0.3 μM ($O_2^{\cdot-}$); DL: 1 μM ((•OH), LR: 0.5–10 μM ($O_2^{\cdot-}$) lower sensitivity to $ONOO^-$, H_2O_2 and ClO^- ;	-Macrophage J774A.1 cells; −Screening of antioxidants: ascorbic acid, p-coumaric acid, quercetin, and α-tocopherol	[28]
Nanoporous Si with 20–30 nm pores, covered by chitosan oligomers with covalently bound DCFH	λ_{exc} = 532 nm, λ_{emm} = 560 nm	Increase in fluorescence due to PON-induced oxidation of DCFH to DCF	Monitoring peroxynitrite–glutathione redox reaction by fluorescence switching	Proof-of –concept of nanoreactor to test reducing and oxidizing agents in real time.	[24]
AuNPs 13 nm	Colorimetric detection at 520 nm	Color change due to PON-induced cleavage of ssDNA adsorbed on NPs and particle aggregation	LR: 9.78–20.77 mM ($ONOO^-$) LR: 3.21–12.8 μM (ascorbic acid).	ascorbic acid, gallic acid and caffeic acid in buffer solutions	[49]

CLIO Cross-linked iron oxide nanoparticles; *DCF* 2′,7′-dichlorofluorescein. *Trp-CD* Tryptophan carbon dots. *CF-SPN* Semiconductor polymer nanoparticles for combined CRET and FRET. *PN-CDs* Phosphorus and nitrogen doped carbon dots (PN-CD.). *GSH–$_{TGA}$–CdTe@ ZnS*: core-shell quantum dots with CdTe core capped with TGA and shell of ZnS capped with GSH (GSH–$_{TGA}$–CdTe@ ZnS). BzSe-Cy: Benzylselenide-tricarbocyanine. IRhB: isopropylrhodamine *B. PFODBT* Poly[2,7-(9,9′-dioctylfluorene)-*alt*-4,7-bis(thiophen-2-yl)benzo-2,1,3-thiadiazole]. Galactosylated graft copolymer of poly(styrene) and poly(ethylene glycol) (PS-g-PEG-Gal). *CRET* Chemiluminescence resonance energy transfer. *FRET* Fluorescence resonance energy transfer. *UCNP* Upconversion nanoparticles. *LRET* Luminescent energy transfer. *LPS* Lipopolysaccharide, *PMA* Phorbol 12-myristate 13-acetate. MacTNP: macrophage-targeted theranostic nanoparticles. *NSET* Nanometal-surface energy transfer, DCFH reduced 2′,7′-dichlorofluorescein AuNC, *UCL* Upconversion luminescence

The principles of these optical methods have been presented in more detail elsewhere [17].

As such, the nanomaterials shown to deliver significant advantages towards the specific PON detection in biological applications, include:

1. thiol capped cadmium telluride CdTe and CdTe@ZnS quantum dots [25]
2. fluorescent carbon dots (CDs) prepared from citric acid (CA) and either ethylenediamine [44] or urea [45]; doped with tryptophan [47], phosphorus and nitrogen [43] used for quantitative detection of PON in spiked serum.
3. polymeric nanoparticles: fluorescent nanoprobes based on polymeric micelles [46] or semiconductor polymer nanoparticles (SPNs, [26, 47]). Polymeric micelles provide an easy way to prepare ratiometric probes which include two different fluorophores and can be moreover appropriately coated (e.g with cell-penetrating peptides, [46]) to achieve PON imaging in the intracellular environment. SPNs, composed of π-conjugated polymers, have excellent photostability and are significantly brighter than QDs or small-molecule fluorophores [26]. In applications requiring multiple functionality, e.g. in theranostics nanoparticles, nanoparticles allowing both complex architectures and easy functionalization are desirable and SPNs appear as preferred starting nanoprobes. [29]
4. rare-earth nanocrystals doped with lanthanides, e. g Yb/Er co-doped hexagonal phase $NaYF_4$ [48] displaying upconversion luminescence (UCL) emission, i.e. having the ability to convert adsorbed light into emitted signal of shorter wavelength e,g near infrared (NIR) radiation into visible light. These 'upconversion nanoparticles" have remarkable chemical/photo stability, and tunable, narrow emission bands. Moreover, the NIR laser used for excitation ensures light penetration depth, no autofluorescence from biological samples [48] as well as no co-excitation of common dyes absorbing in the UV/visible region, thus UCNP are suitable to act as energy donors for luminescent energy transfer (LRET) based nanoprobes [48].
5. amphiphilic, macrophage-targeted theranostic nanoparticles (MacTNP), self-assembled from a Chlorine6 (Ce6)-hyaluronic acid (HA) conjugate [29].
6. biocompatible cross-linked iron oxide (CLIO) nanoparticles, commercially available, adapted for ROS-detection by labeling with oxazine fluorophores [28].
7. metallic (Au) nanoparticles, whether unmodified [49] or coated with fluorophores [27]. These were useful for the screening of PON-scavenging antioxidants in buffers [49]), for instance by taking advantage of the easiness of modification of AuNPs with DNA and of colorimetric detection of aggregated Au NPs. In this type of assay, the antioxidant effect is associated with a compounds' capability to prevent peroxynitrite-induced DNA damage. Hybrid Au-Si nanoparticle complexes such as dye-encapsulated silica particles decorated with satellite AuNCs have also been used for PON detection, forming a dual emission fluorescent nanocomplex (e.g. [24]). Metallic NPs present strong and stable fluorescent signals in the NIR range and no photo-bleaching. ROS, including PON may quench the intrinsic fluorescence of Au nanoclusters [24] thus appropriately designed nanoprobes decorated with Au nanoclusters are efficient for imaging ROS inside the cells [24]. Alternatively, modification of AuNPs by different surface chemistry approaches were used to alter their fluorescence properties and selectivity towards particular ROS [16].
8. fluorophore-modified nanoporous silicon, investigated as a nanoreactor for studying redox processes involving PON [23].

The selection of nanomaterial for PON imaging is related to specific requirements of each application and strategy used for optical detection as detailed in the next section. The probes should display appropriate linear range, sensitivity and response time as required for reporting variations in PON fluxes at physiologically relevant levels. Moreover, the tissue penetration depth is critical when designing nanoprobes for in vivo applications. Near IR emitting probes are a prerequisite for imaging PON in deep tissues and living animals, to avoid the auto fluorescence of biological samples. In vivo imaging of PON and ClO^- was achieved for example with SPN by monitoring the fluorescence ratio I680/I820 nm [47]. Whenever the envisaged detection strategies involve energy-transfer mechanisms such as NSET, FRET, CRET or FRET, good materials to consider are AuNPs, UCNPs and SPNs, respectively. Reversibility of the signal is also important to report on dynamics of PON fluxes.

Strategies for optical detection of PON

The main mechanisms by which optical detection of PON is achieved with nanomaterial-based systems are: (1) color change of NP suspensions following PON-induced aggregation, (2) fluorescence quenching, (3) fluorescence activation and (4) fluorescence recovery (de-quenching) by PON.

Color change of NP suspensions following PON-induced aggregation

Being a strong oxidizing and nitrating agent, PON can induce DNA modification and cleavage of DNA strands in physiological conditions. As shown [49], colorimetric detection based on Au NPs provides fast and sensitive assessment of DNA damage in vitro and is adapted for the screening of

antioxidants protect against such damage. The principle of detection relies on adsorption of ssDNA on Au NP_S and the cleaving of DNA by PON and other ROS. Intact adsorbed DNA strands on AuNPs prevent particle aggregation indue to electrostatic repulsion between particles coated with negatively-charged DNA. Instead, fragmented DNA cannot offer protection against NPs aggregation (Fig. 8).

Particle aggregation induced by PON translates into a color change of NP solution, visible with the bare eyes, from red (non-aggregated nanoparticles) to blue (aggregated nanoparticles) and the effect is correlated with the concentration of PON/ROS and antioxidants in solution. This principle was applied to study the PON scavenging effect of ascorbic acid, gallic acid and caffeic acid in vitro [49] and would be amenable to application in screening antioxidant drugs in vitro in buffers of controlled, low ionic strength. Moreover, this method provides a simple, fast and economic way to visualize one of the cellular effects of PON, namely DNA damage; however it would not be appropriate for real time monitoring of PON concentration or for cellular assays.

Fluorescence quenching

Whereas a panel of ratiometric probes have been developed harnessing the differential reactivity of dyes selective toward $OONO^-$ [50–53], the use of nanomaterials has brought new valences to the concept. For example, embedding the hydrophobic indicator dye benzyl selenide tricarbocyanine BzSe-Cy [46] in a carefully designed polymeric micelle has allowed improving the selectivity for PON compared to the free dye and achieving ratiometric imaging of intracellular PON in phagocytic and non-phagocytic cells [46]. At the core of nanoprobes selectivity lays the specific oxidation of divalent selenium in the NIR-fluorescent dye BzSe-Cy to quadrivalent selenium as depicted in Fig. 9. The oxidized dye displays only weak fluorescence and the degree of fluorescence quenching is linearly correlated with PON concentration in the range 0–5 μM, when measured at room temperature in 0.1 M phosphate buffer saline (PBS) pH 7.4. Remarkably, the selenium oxidation reaction and corresponding fluorescence quenching effect on BzSe-Cy can be reverted, e.g. by reduction with ascorbate providing the basis for detection of dynamic PON

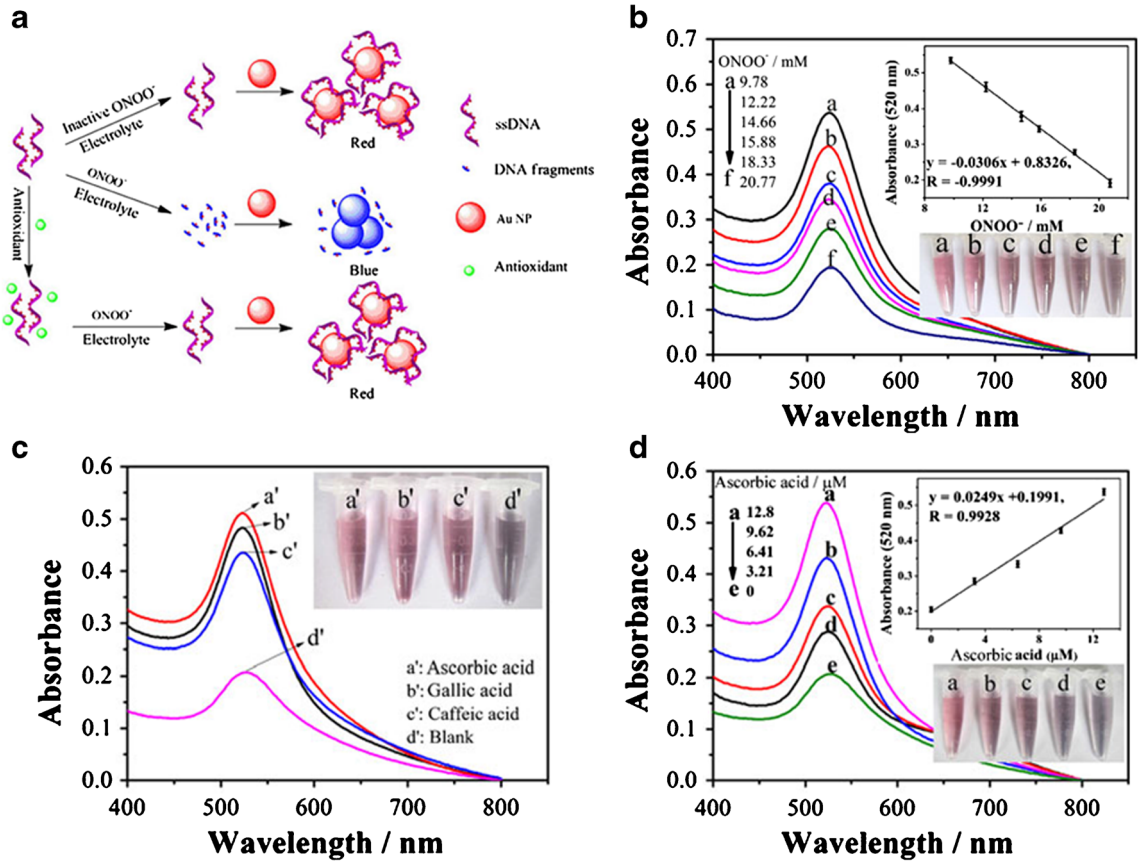

Fig. 8 (**a**) Schematic representation of the colorimetric assay for DNA damage detection. (**b**) Absorption spectra of AuNPs in the presence of 0.06 μM ssDNA-1 and different concentrations of ONOO− , after incubation at at 37 °C for 10 min. (Inset: Correlation between absorbance at 520 nm and concentration of ONOO− in solution, as well as corresponding colors of the solutions). (**c**) Absorption spectra and color changes (inset) of a solution of AuNPs/ssDNA-1 incubated with 21.7 mM ONOO− in the absence (blank) or presence of 12.8 μM of various antioxidants. (**d**) Exemplification of colorimetric assay presented in (**c**) for detection of ascorbic acid: solution absorption spectra, color changes (inset) for different concentrations of ascorbic acid and calibration curve (inset). Reproduced from [47] with permission from Springer

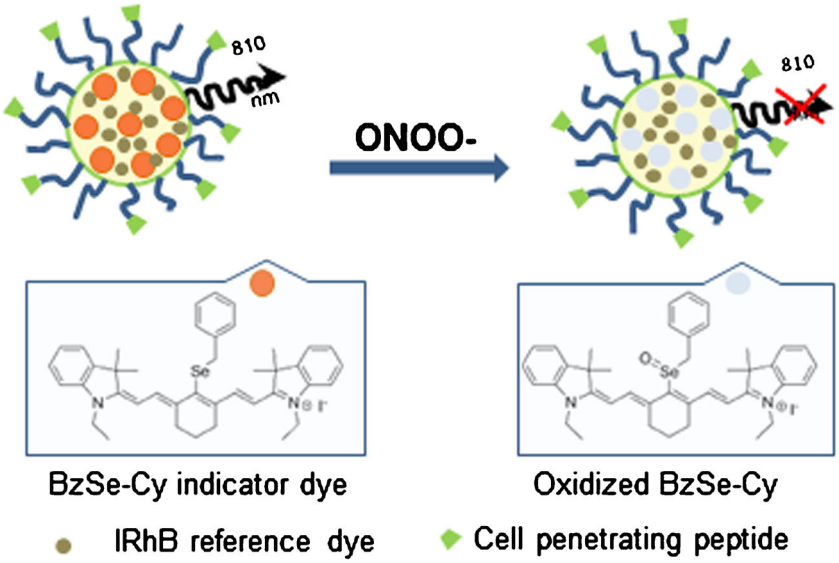

Fig. 9 Fluorescence quenching by PON, redrawn based on the concept presented in [44]

signaling. Nevertheless, the approach, although appealing, has limited applicability for in vivo assays. While redox cycling of free BzSe-Cy in vitro and its use for real-time imaging of redox cycles in macrophage cells were successfully demonstrated [54], the reversibility of fluorescence signal of the micelle-embedded dye remains yet to be proven.

Fluorescence activation

According to certain design strategies, through its oxidative action, PON cleaves the bonds within nanomaterials-attached non fluorescent small molecules, leading to the release of fluorescent compounds. Alternatively, PON oxidizes the non-fluorescent, reduced form of a fluorophore, attached to a nanomaterial, into a strongly fluorescent oxidation product that remains bound to its support, enabling precise localization and targeting. Both alternatives have gained applicability in bioimaging applications. For example, the surface of biocompatible magnetic nanoparticles was modified with an oxazine-based non-fluorescent derivative via covalent attachment by carbodiimide chemistry. Chemical cleavage by PON and other ROS triggered the release of small oxazine fluorophores showing strong NIR fluorescence [28] (Fig. 10). Such mechanism, being based on irreversible transformations induced by PON, cannot be used to image the dynamics of PON fluxes yet it is useful to capture high quality images of PON and other ROS- producing events. In a different approach, oxidation by PON of the nonfluorescent reduced form of dichlorofluorescein, covalently fixed on nanoporous silicon results in formation of a strongly fluorescent oxidation product. The fluorophore remains attached to the nanoporous support [23] and the redox reaction is reversed with glutathione (GSH). A second exposure to PON leads again to an increase in the fluorescence signal, although smaller than observed initially. Thus, the nanostructured porous silicon chip functionalized with dichlorofluorescein is considered as proof-of concept for a nanoreactor responding to ROS and for the dynamic study of redox reactions. Improvement of experimental setup and conditions to prove reversibility of PON-responsive system through multiple dye oxidation/reduction steps, i.e. fluorescence on/off cycles will further advance this concept. Translation of this concept into a nanoparticle probe for real-time in vivo imaging has not yet been reported. Designing nanoparticles modified in a similar manner as above, with a NIR-fluorescent dye remains as a challenge for the future.

Fluorescence recovery (de-quenching)

In some ingeniously designed nanostructures, the inherent fluorescence of nanomaterials was quenched due to energy transfer to nearby immobilized fluorophores. Examples of energy transfer phenomena used for quenching nanomaterial's fluorescence include: FRET from SPN to fluorophores [26, 47], NSET from Au NP to fluorescein [27] and LRET between UCNP and Rhodamine B [48].

The mechanism for detecting PON and other ROS based on fluorescence recovery of nanoprobes relies on the oxidizing power of the free reactive species which cleave the link between nanomaterials and acceptor fluorophores, abolishing the energy transfer to restore nanomaterial's inherent fluorescence or luminescence. The success of these strategies relies on adequate choice of donor and acceptor molecules based on their absorption and emission maxima, as well as on efficient immobilization of the acceptor molecules in the close vicinity of energy donors [26] [26]. For example, the NanoDRONE system consists in a RONS-inert, NH_2-functionalised SPN core acting as energy donor, coated with a RONS-sensitive fluorophore, IR775COOH, via carbodiimide chemistry. The

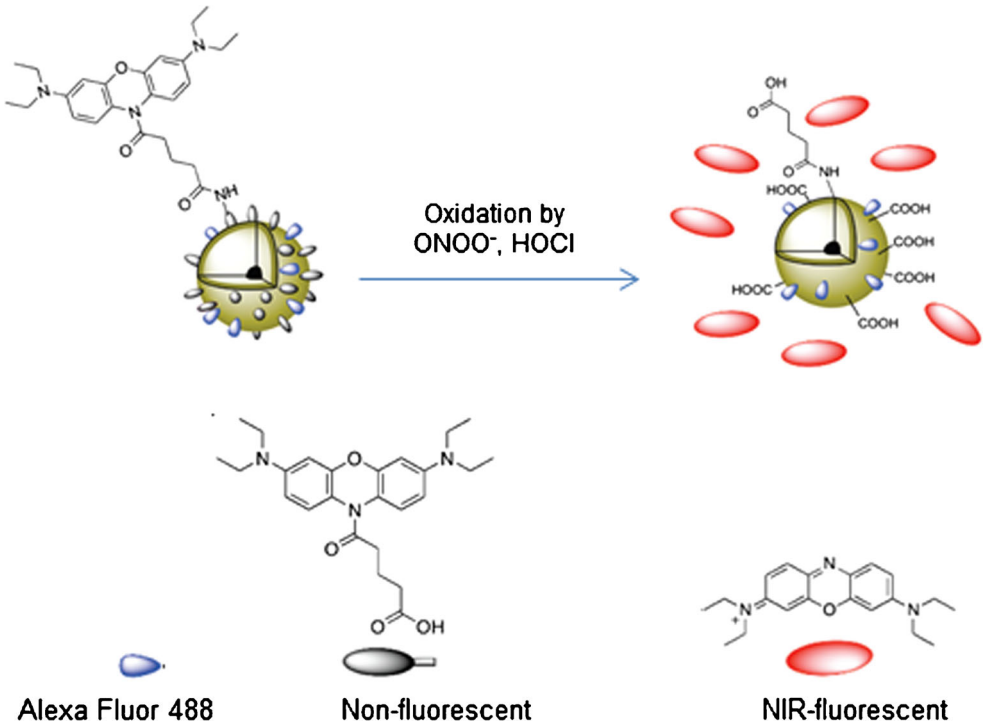

Fig. 10 Illustration of fluorescence de-quenching (activation) of oxazine-modified NPs by PON and HOCl. Adapted from [28], with permission from the American Chemical Society

spherical SPNs were prepared by nanoprecipitation and include a fluorescent polymer and two PEG-ylated matrix polymers, from which one with amino functional groups, allowing immobilization of IR775COOH fluorophore on the SPN. The fluorescent polymer from the SPN core has an emission maximum at 678 nm while IR775COOH has absorption maximum at 788 nm and emission at 818 nm. Oxidative cleavage of the oligomethine moiety of the fluorophore IR775COOH by PON and other ROS leads to cancelation of FRET from the SPN and recovery of the SPN fluorescence signal at 678 nm (Fig. 11) [26].

In another approach, Lee et al. [27] used a bio-inspired strategy to immobilize fluorescein labeled HA molecules on Au NPs of 16 nm size, via strong Au-catechol interactions. The length of HA chain (15 nm for an average molecular weight of 5600 Da HA) was selected as to achieve efficient NSET between AuNPs and the fluorophore. The selective degradation of HA chain by PON and other ROS resulted in the release of fluorescein-labeled HA fragments and abolishment of NSET from Au NPs to fluorescein. Consequently, the fluorescence of AuNPs was turned "on" (Fig. 12) [27].

Alternatively, Rhodamine B-labeled HA was covalently immobilized on the surface of UCNP by carbodiimide chemistry. UCNPs present green luminescence emission bands at 515–534 nm and 534–560 nm as well as red emission at 630–680 nm, while Rhodamine B has broad absorbance with the maximum at 552 nm and luminescence emission at 572 nm, which doesn't overlap with the red emission of UCNPs. LRET occurs between the green emission bands of UCNP and Rhodamine B [48]. When ROS cleaves the HA chains in UCNP coated with Rhodamine B-decorated HA, it cancels LRET from UCNP to Rhodamine B and the green luminescence signal of UCNP is restored (Fig. 13) [48].

Approaches to ensure optimum detection characteristics for PON by nanomaterial-based optical methods

Nanomaterials allow rich possibilities when designing nanoprobes for PON and other reactive species for specific imaging applications and tuning them to display ideal characteristics pertaining to: (1) spatial and temporal resolution; (2) sensitivity; (3) specificity/selectivity; (4) stability in the measurement medium and resistance to photo- and chemical bleaching; (5) biocompatibility, bioavailability and tissue penetration depth; (6) pharmacokinetics.

Spatial and temporal resolution

Appropriate spatial and temporal resolution are mandatory for real-time imaging of PON bursts and GSH reparation, in order to understand the physiological and pathological roles of PON and pinpoint the precise intracellular location of nanoprobes used to report on PON. Whereas the size, surface charge and surface functionalization are in general critical characteristics to control optical imaging with nanoprobes [19, 31] worth analyzing is the specific nanoprobe design to achieve high spatial contrast and resolution for PON detection and warrant efficient delivery to targeted areas and optimum local concentration of fluorescent reporter(s). As demonstrated for imaging of intracellular peroxynitrite produced in phagocytic and non-

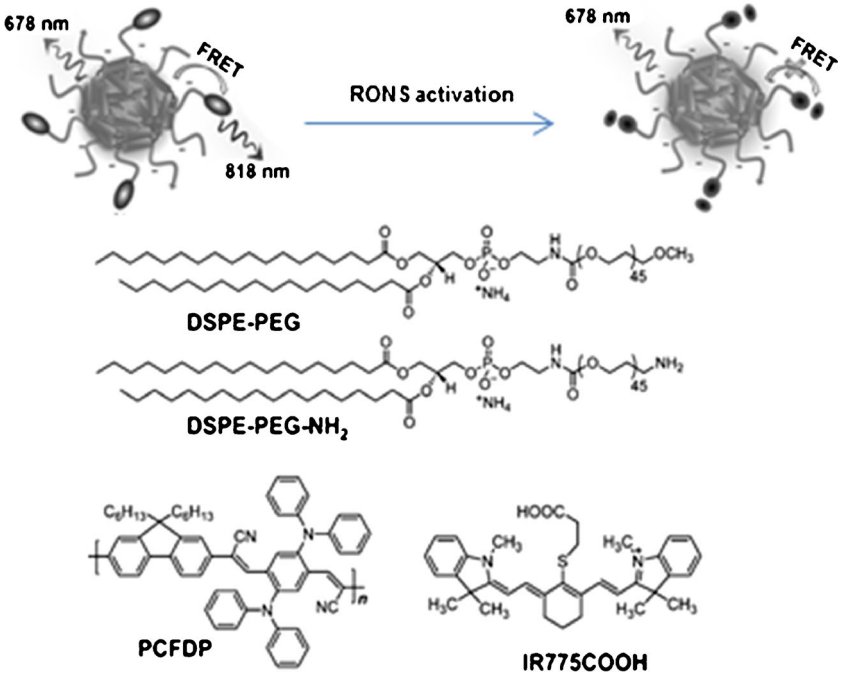

Fig. 11 RONS sensing scheme with NanoDRONEs, and the structures of the four components: PCFDP, DSPE-PEG, DSPE-PEG-NH2 and IR775COOH. More explanations are provided in the text. Reproduced in part from [26] with permission from Wiley

phagocytic cells, the premises for high quality imaging are created by inclusion in the same nanoprobe of two fluorescent reporters for ratiometric detection, coupled with protection against photobleaching and chemical degradation and with selection of excitation and emission wavelength that ensures low background. Such a cell-permeable nanoprobe consisting in a polymeric micelle coated with cell-penetrating peptides and incorporating two dyes for ratiometric and highly selective detection has been reported [46]. As per another strategy, imaging of PON, ClO− and •OH was achieved with SPNs having a modular core-shell design, where FRET was allowed from a fluorescence matrix polymer in the SPN core to a second fluorophore, fixed to the SPN surface. Ratiometric detection based on signals corresponding to the two fluorescent reporters provided increased spatial resolution for the real-time tracking of probes in vivo and monitoring ROS at inflammation sites [26] in mice infected with *Corynebacterium bovis* (Fig. 14). In the absence of ROS, the nanoprobes location in vivo was identified thanks to the fluorophore IR775COOH emission signal due to FRET. In the presence of PON, activated probes displayed increased fluorescence intensity of the PCFDP polymer due to abolishment of FRET.

Similar PEG-ylated SPNs of 50 nm size, encapsulating a chemiluminescence donor and including galactose functional groups for liver targeting were used to image drug-induced hepatotoxicity within minutes of drug challenge, as a dose-dependent ROS activity in the liver [47]. Ratiometric fluorescence detection was used for imaging PON and ClO− while H_2O_2 was detected by chemiluminescence. The timescale of observations sets apart these nanosensors from methods used to evaluate rather the consequences of radical release all along the chain of events linking RNS/ROS production to hepatotoxicity, such as histological changes, protein nitration and DNA damage. In another report, 50 nm upconversion nanoparticles of Yb/Er co-doped NaYF4 functionalised with hyaluronic acid and Rhodamine B were used to acquire

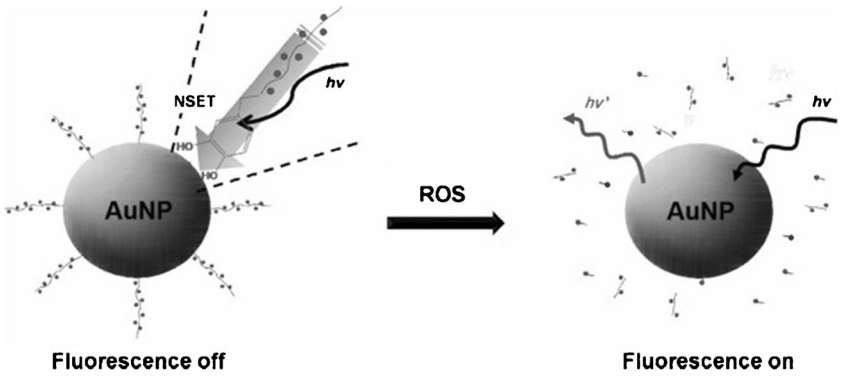

Fig. 12 Fluorescence recovery induced by ROS through the abolishment of NP energy transfer (NSET) in gold nanoprobe with immobilised fluorescein-HA. Reproduced from [27] with permission from Wiley

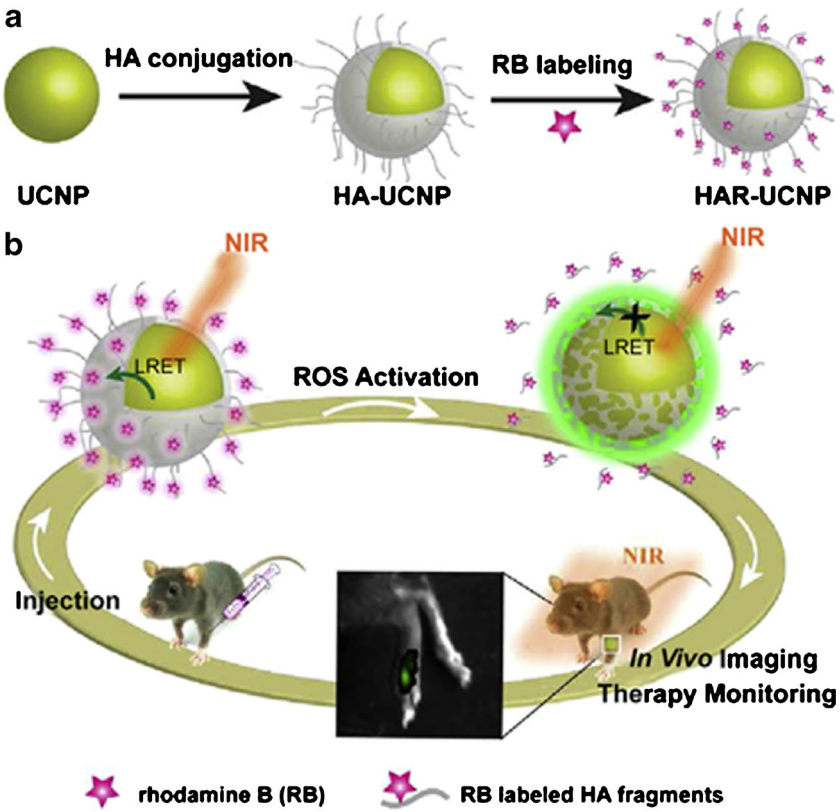

Fig. 13 (**a**) Production of HAR-UCNP nanoprobes for diagnosis of rheumatoid arthritis in mice, by conjugation of UCNP nanoprobes with hyaluronic acid (HA) and subsequent labeling with Rhodamine B. The functional properties of HAR-UCNPs are due to Rhodamin B acting as LRET acceptor from UCNP, and to HA, conferring sensitivity to ROS, water solubility and biocompatibility (**b**) Schematic representation of the LRET process of HAR-UCNPs involved in ROS detection for diagnosis and therapy monitoring of rheumatoid arthritis. Reproduced from [46] with permission from Elsevier

luminescence images of arthritic areas in limbs of healthy mice, arthritic mice and mice treated with methotrexate (an anti-arthritis drug), allowing for both diagnosis of rheumatoid arthritis and therapy monitoring [48].

i. Sensitivity

Heightened sensitivity for PON detection and imaging by nanomaterial-based optical methods was achieved based on a combination between:

- **ratiometric detection** for better imaging contrast and accuracy. With most nanoprobes the net optical signal is expressed as the ratio of signal intensity recorded at two emission wavelengths, one correlated with PON presence and a second one which is insensitive to PON and serves as a reference. The reference signal allows to compensate for variations in local nanoparticle concentrations or for small variations in excitation intensity, as well as to evaluate the progress of intracellular delivery. This approach was typically achieved using two dyes incorporated in the same micelle nanoparticle [46], with two nanomaterials linked in a nanocomplex, a dye-incorporating silica and Au nanocrystals [24] or with one matrix fluorescent polymer and a surface-bound fluorescent PON-indicator dye linked in a SPN [47].
- **low background fluorescence** signal as result of NIR emission (650–900 nm) [26, 46–48], avoiding the auto fluorescence of biological tissues and achieving accurate detection of PON in vivo.
- **signal amplification** through fragmentation of ligand chain –e.g. in the case of nanoparticles linked to HA.
- **optimized size, nature and surface chemical modification** of NPs. For example higher quenching by PON was found with CdTe QDs compared to CdS QDs due to the nanocrystal (NC)–thiolate bond being stronger for CdS than for CdTe. Furthermore, coating of the core with a higher bandgap material such as ZnS (3.7 eV) and modifying the surface with various thiols also improved the sensitivity of QDs [25]. Nevertheless, the inherent cytotoxicity of QDs is one of the drawbacks of this approach.

ii. Specificity/Selectivity

Selectivity is crucial for ensuring accurate assessment and interpretation of PON levels and their variations. Reaching good selectivity in a particular application can be facilitated by a combined approach considering: (i) PON-specific fluorescent probes and (ii) nanoprobe design and the mechanism of activation, upon PON action, of the reporter probe responsible for optical detection, with minimal interference from other reactive species.

PON-specific fluorescent probes There are increased efforts to synthesize small molecule fluorescent probes with higher

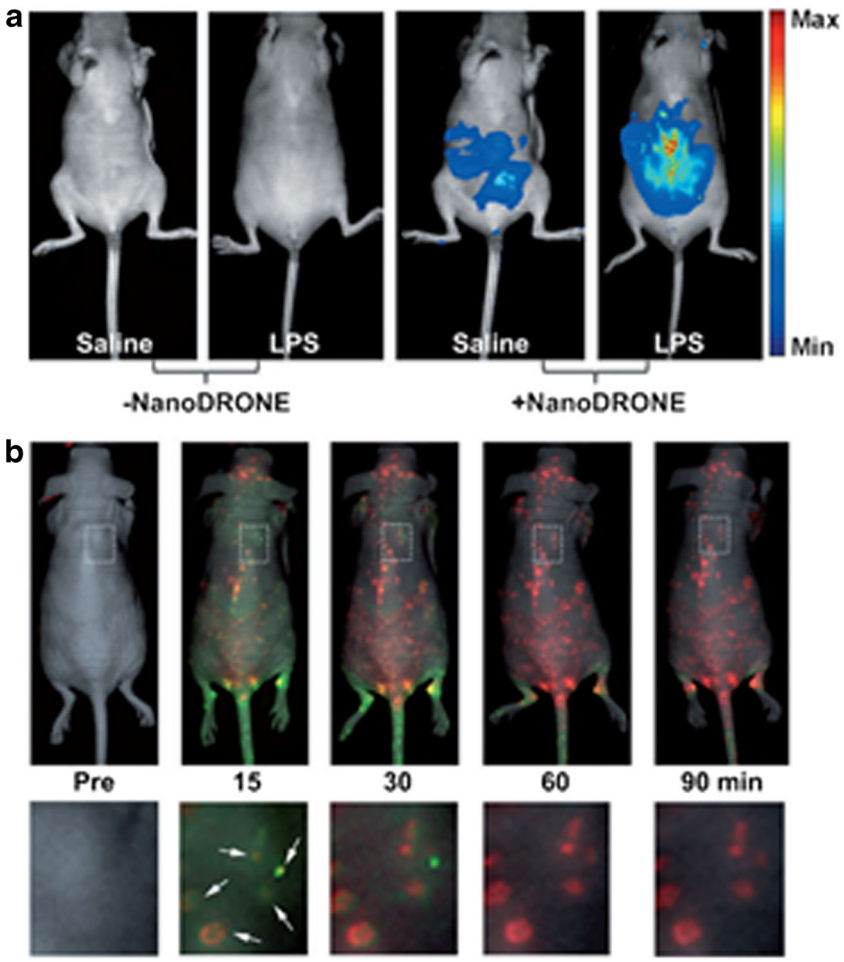

Fig. 14 **a** In vivo imaging of RONS in a LPS-induced acute peritonitis mouse model before and 30 min after administration of NanoDRONEs. Saline ($n = 4$) and LPS ($n = 4$) were administered 4 h later before administration of NanoDRONE. **b** Overlaid images of activated (red) and inactive (green) NanoDRONE for imaging RONS in mice with spontaneous systemic *C. bovis* infection ($n = 4$). The images on the bottom raw represent enlargements of corresponding regions indicated by white boxes in images above. White arrows point to local areas of bacterial infection. Reproduced from [26] with permission from Wiley

specificity for PON [1, 51, 53] to be integrated within nanomaterials for even better selectivity. In line with this goal, new molecules have been produced that are either oxidized or nitrated by PON. Their sensitivity to PON is triggered by oxidative or nitrating/nitrosating mechanisms [51], including oxidation of activated ketone (*e.g* HK-Green 1 to HK-Green 3); oxidation of organoselenium fluorophores (e.g Cy-PSe and Cy-NTe [52]); oxidation of phenol coupled to other oxidative mechanism (e.g. PN600), oxidation and cleavage of spiro xanthene derivatives from non-fluorescent spiro closed forms to fluorescent spiro open forms (e.g Rhodamine B Phenyl Hydrazide (RBPH) and boronate oxidation, a genetically encoded fluorescent probe that contains a p-boronophenylalanine derived chromophore [51]). Other fluorescent probes relied on nitration of the aromatic ring (e.g NiSPY-3) or nucleophilic nitrosation of secondary amine (e.g. Ds-DAB-N-(2-aminophenyl)-5-(dimethylamino)-1-naphthalenesulfonic amide).

A remarkable example is benzylselenide-tricarbocyanine (BzSe-Cy) [54], whose selectivity for PON was further improved upon encapsulation in a polymeric micelle [46]. The fluorescence of micelle-incorporated dye is quenched by PON in a dose-dependent manner (Fig. 15a), as per the mechanism discussed in section 4.3.2. Selectivity for PON was proven by comparing the signal for 5 μM for $ONOO^-$ which causes to 96% decrease in F810/F575 fluorescence ratio with 500 μM for H_2O_2, $^1O_2$, $O_2^{\bullet-}$, CNO, NO_2^-, NO_3^-, and $ROO^{\cdot}$, 450 μM for $CO^{\cdot}$, 250 μM for ClO^- and 10 μM for HRP. All other ROS, including highly active ones such as ClO^- and •OH, did not interfere with PON, i.e. caused less than 5% change in F810/F575 fluorescence ratio (Fig. 15b). Moreover, the selectivity and usefulness of the new nanoprobe was illustrated through in vitro testing of 3 cellular lines, including RAW 264.7 macrophages and HL-7702 and HepG2 cells non-phagocytic cells [46]. In these experiments, the fluorescence signal decreased only in cells challenged with the PON donor SIN-1 and not in those treated with a •NO donor, S-nitroso-N-acetyl-DL-penicillamine (SNAP) or a $O_2^{\bullet-}$ donor, xanthine/xanthine oxidase, thus proving that the signal measured with the probe was due exclusively to PON (Fig. 15 c).The good selectivity of the nanoprobe based on the BzSe-Cy dye is due to a synergetic effect between the selectivity of free dye and properties of the nanomatrix, as explained below.

In some cases, simultaneous and accurate detection of several other reactive species besides PON is desired in order to shed light on the ROS fluxes in the biological processes investigated. For example, monitoring of both ClO^- and PON is

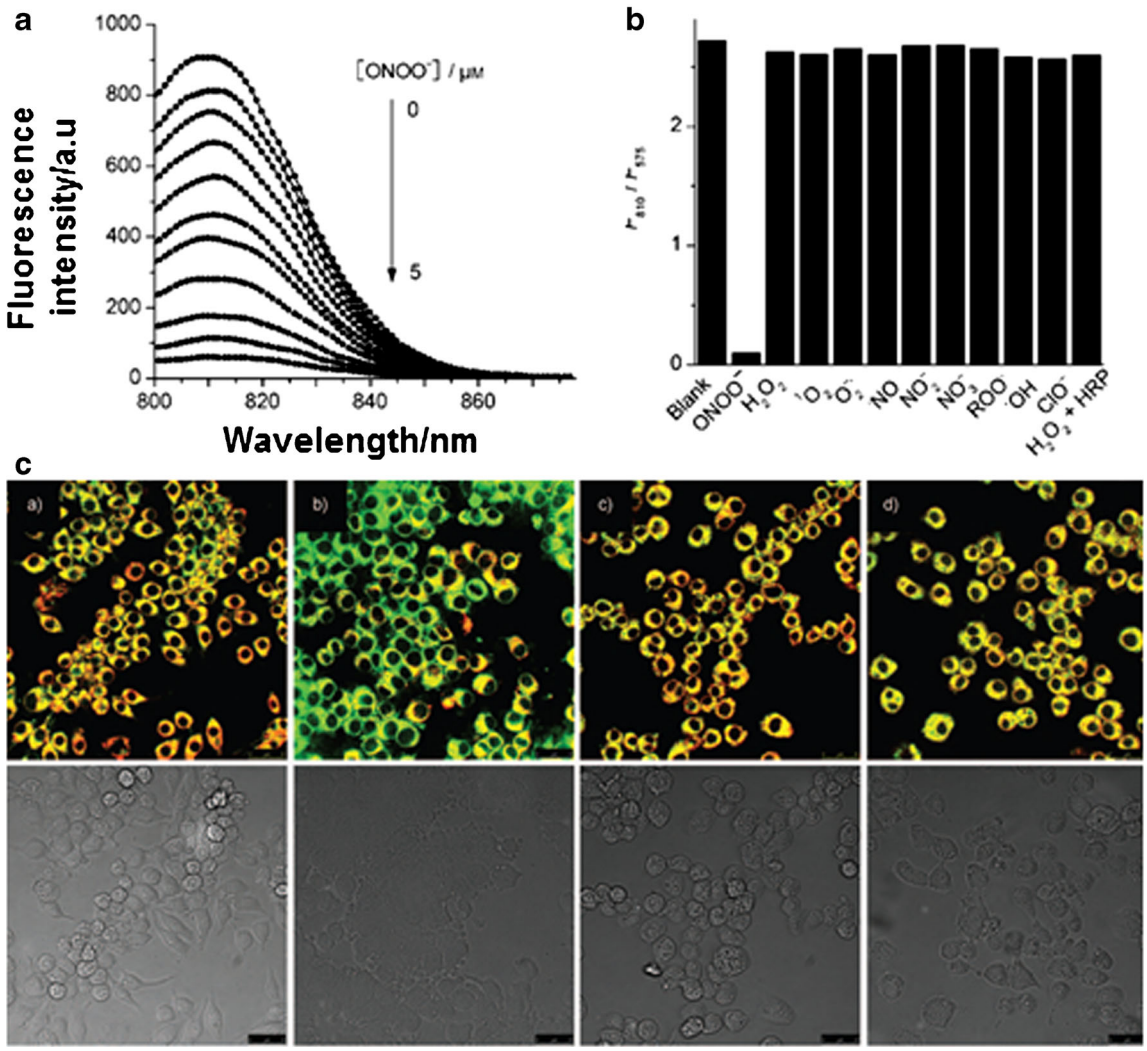

Fig. 15 **a** Fluorescence signal of the nanoprobe recorded at various concentration of $ONOO^-$ (from top to bottom: of 0; 0.05; 1; 1.5;2;2.5;3;3.5;4;4.5 and 5.0 μm). The spectra were recorded at room temperature in 0.1 M PBS pH 7.4, with excitation at 788 nm. **b** Fluorescence signal ratio F810/F575 ratio of the nanoprobe (0.25 mg/mL, in 0.1 M PBS) with various analytes: 5 μM $ONOO^-$, 500 μM for H_2O_2, $^1O_2$, $O_2^{\cdot-}$, NO, NO_2^-, NO_3^- and $ROO^{\cdot}$, 450 μM for $^{\cdot}OH$, 250 μM for ClO^- and 10 μM for H_2O_2 + HRP. (**c**) Confocal fluorescence images of RAW 264.7 macrophage cells acquired with the nanoprobes. Top: images, displayed in pseudocolor, represent the ratio of emission intensities collected in of the 700–800 nm(red) and 535–600 nm (green) domains,. Bottom: images obtained in bright-field. To investigate selectivity, the macrophage cells, pre-incubated with 0.03 mg/mL nanoprobes for 60 min at 37 C were challenged with (from left to right). (i) control; (ii) 10 μM SIN-1; (iii) 10 μM SNAP and (iv) 100 μM xanthine and 0.1 U of xanthine oxidase. Scale bar: 25 μm. Reproduced from [44] with permission from Wiley

highly relevant for understanding the chain of events associated with ischemia/reperfusion [55, 56]. A coumarin derivative, PN600 was reported to act as a three channel fluorescent probe allowing accurate detection of ClO^- and PON [53], and is anticipated that its applications with nanomaterials will be explored in the future.

Nanoprobe design In addition to the inherent properties of the free dye and the use of ratiometric detection to alleviate some interference from other reactive species, the mechanism of activation of the reporter probe by PON provides an alternative path to achieve selectivity of detection. The design of the probe is paramount for ensuring selectivity towards PON and several possibilities have been explored so far, to:

- adapt the nanomatrix to act as a diffusion barrier for interfering reactive species and larger analytes modulates the selectivity of nanoprobes for PON. This was achieved for example by encapsulation of a PON-indicator dye and a reference dye in the hydrophobic core of a polymeric micelle [46]. The hydrophobic core made of poly(D, L lactic acid) (PLA) is surrounded by a hydrophilic shell consisting of polyethylene glycol (PEG), conjugated to cell penetrating peptides. This design allowed a significant gain in selectivity over the free, non-encapsulated dye,

attributed by the authors to the protective effect of the nanomatrix: compared to PON, other ROS (e.g $O_2^{\bullet-}$ and ClO^-) have lower diffusibility or shorter lifetime (e.g •OH), whereas some other potential interfering compounds have larger sizes that do not allow them to permeate into the nanomatrix[43. Such an approach, where nanomaterials add diffusional barriers to filter out possible interferents while being also functionalized with an outer layer of cell penetrating peptides or with groups ensuring targeted delivery, can be envisaged with other fluorescent probes sensitive for PON as well.

- adapt the nature and surface chemistry of core-shell quantum dots: coating CdTe and CdSe QDs with thiols such as 3-mercaptopropionic acid (MPA), thioglycolic acid (TGA), or glutathione (GSH) enhanced their selectivity towards PON[26]. The best selectivity was displayed by core-shell quantum dots with CdTe core capped with TGA and shell of ZnS capped with GSH (GSH_{-TGA}–CdTe@ ZnS), possibly thanks to the affinity of PON for GSH and to steric restrictions prompted by the size of the GSH [25].
- ROS-induced fragmentation of hyaluronan (HA), a high molecular weight polysaccharide, component of synovial fluid with relevance for the progress of rheumathoid arthritis [57–59]. Cleavage of HA was exploited in the design of nanoparticle-based systems for the optical readout of intracellular processes involving PON and other ROS, where HA was used as a ligand. The degree of selectivity towards PON compared to other highly reactive species with known ability to fragment HA such as $O_2^{\bullet-}$, •OH and ClO^- depends on the design and the nature of the probe. For example, 15 nm-long HA with average molecular weight of 5 kDa, conjugated with fluorescein and immobilised on AuNPs was degraded with higher sensitivity by superoxide anion ($O_2^{\bullet-}$) and hydroxyl radical (•OH) [27] as compared to PON and other ROS. Upconversion luminescent NPs of 50 nm size, modified with 40 kDa HA and then linked to Rhodamine B presented similar detection limits of 0.03, 0.02, 0.06 and 0.1 mM for •OH, ClO^-, ONOO- and $O_2^{\bullet-}$, respectively [48]. Good selectivity to PON was observed for the cleavage of amphiphilic nanoparticles of 103 nm hydrodynamic size, self-assembled from a fluorophore, Chlorin e6, conjugated with HA of 215 kDa MW. Restoration of Chlorin e6 fluorescence due to ROS-induced degradation of HA was observed most sensitively for PON, compared to $O_2^{\bullet-}$,•OH, H_2O_2 or ClO^- [29].

iii. Stability and resistance to bleaching

Good stability in the measurement medium is paramount for practical applications of PON nanoprobes. Many of the developed nanoprobes displayed adequate stability in a wide range of pH and ionic strength buffers and in cell culture media, without showing aggregation, degradation or dye leakage [24, 27, 46]. Common design approaches to avoid leakage of the fluorescent dye include covalent immobilization of the dye to the nanoparticle [24] or encapsulation into polymeric micelles [46]. Aqueous dispersions of hybrid nanoprobes obtained by encapsulation of organic fluorescent dyes into polymeric micelles, followed by nanoparticle coating with cell penetrating peptides, were found to be stable for at least 80 h, with less than 1% dye leakage at pH 7.4 over this time period [46]. Stability of fluorescein-HA conjugated Au nanoparticles against glutathione, under intracellular reducing condition was ensured by employing dopamine as anchor for the immobilization of HA onto the surface of AuNPs [27].

An additional advantage of incorporating fluorescent probe in a nanomatrix is the resulting stabilization of the probe against photon-induced chemical damage [46]. Not in the least, choosing the adequate nanomaterial type is important to avoid chemical bleaching of the reporter probe as ROS and RNS present in the microenvironment in vivo might degrade the fluorescent probe. For instance, one advantage of semiconductor polymer nanoparticles over quantum dots and small molecule fluorophores is their highly superior resistance to oxidative chemical bleaching effects by ROS and RNS [47].

iv. Biocompatibility and cytotoxicity

Biocompatibility is defined by IUPAC (International Union of Pure and Applied Chemistry) as the "ability to be in contact with a living system without producing an adverse effect." The nature, size, surface chemistry and surface charge determine the biocompatibility and the efficient and targeted delivery of optical probes in complex biological environments. Optical nanoprobes can bind non-specifically to proteins and cellular membranes and as consequence will not reach the areas targeted for imaging. Carbon dots represent a notable exception: these are stable clusters of carbon atoms with diameters of typically 2 to 8 nm, biocompatible (i.e., not harmful to cells and tissue within a few days and not known to be toxic), cell permeable, easily excreted, weakly interacting with proteins, and invisible for the immune system. Typically, to avoid non-specific binding of proteins and ensure biocompatibility, nanoparticle-based optical probes are coated with polyethylene glycol (PEG), a hydrophilic polymer with high conformational flexibility and an almost neutral charge. However, PEGylated nanoprobes display significantly greater hydrodynamic diameters compared to the unmodified ones and in some cases the increased size prevents them from entering cellular structures. An alternative to PEG is the modification with multidentate polymer ligands containing hydroxyl groups. These were shown to wrap tightly around QDs and protect them efficiently against non-specific binding in biological media, while minimising particle size [31].

Efficient and targeted delivery of nanoprobes for PON imaging was achieved by tuning probe composition and coating. For example, to ensure their access to intracellular space and endosomal escape polymeric micelles were coated with cell-penetrating peptides [24, 46]. In another example, delivery of SPNs to the liver [47] was ensured via galactose groups, by including in the composition of SPNs a galactosylated graft copolymer of poly(styrene) and poly(ethylene glycol) [47]. These SPNs measuring around 55 nm and containing both a chemiluminescence-reagent sensitive to H_2O_2 and a fluorescent dye sensitive to PON and ClO^- were successfully employed for hepatotoxicity testing and repair [47]. Besides targeted delivery, the mechanism of passive delivery based on the EPR effect is largely used for imagining tumor and inflammation sites. By this strategy, systemically administrated, 78 nm PEG-coated SPNs (called "NanoDRONEs") were delivered at inflammation sites due to leaky vasculature in inflammation areas and high uptake of PEG-protected nanoprobes. The "NanoDRONEs" were thus used for imaging RONS in mice with spontaneous systemic *C. bovis* bacterial infection [26]. Risk assessment of nanomaterial-based probes needs to be performed on a case-by-case basis. Most PON probes detailed in Table 2 displayed no cytotoxicity, as tested through cell viability tests, typically by the MTT (3-(4,5-dimethylthiazol-2-yl)-2,5-diphenyltetrazolium bromide) tetrazolium reduction assay [24, 43, 46] using normal rat kidney cells. There are different mechanisms by which cytotoxicity occurs [60] and little is yet known about the effect of the probes on the system that will be imaged –being this cells, tissues or whole animal.

v. Pharmacokinetics

Long blood circulation time and adequate clearance from the body are bottlenecks for the application of imaging probes in the biomedical field. To reach the necessary local concentration of nanoprobes at tumor sites for high quality imaging, the nanoprobes need to evade fast clearance from the blood stream by defense systems (reticuloendothelial system, RES - and mononuclear phagocytic system MPS) which lead to nanoparticle accumulations in liver and spleen. Size, surface coating and charge are determining factors of nanoprobes' interaction with living systems. Typically, the nanoprobes used for imaging have hydrodynamic diameters larger than 20 nm and PON detection is no exception (Table 2). While the renal clearance of neutral QDs with diameter smaller than 5.5 nm was demonstrated, upon systemic administration, larger nanoprobes are rapidly taken by the MPS system, cleared from the bloodstream and accumulated in the liver. The same scenario happens when the nanoprobe's surface charge and coating does not prevent non-specific binding to blood proteins and cellular membranes (see section 4.4.5). When all these difficulties are prevented by smart probe design (size, charge, composition and coating) the benefits of nanomaterials, compared to small molecule reporters with regards to pharmacokinetics and bioimaging are obvious. By attachment of fluorogenic oxazine groups to biocompatible dextran-coated iron oxide nanoparticles, the blood half-life of oxazine probe for PON and HOCl imaging increased from ~40 min for the small molecule probe to >9 h for the 41 nm nanoparticle probe [28]. Moreover, as each such nanoprobe contained around 400 oxazine groups, the concentration of fluorescent reporter at targeted site was appropriate for quality imaging of ischemia and inflammation in myocardial infarction in mouse. Another study reported that blood circulation half-life of 78 nm SPNs called "NanoDRONEs" was 6 h [26] and the probes presented a favorable biodistribution, i.e.–their accumulation in liver and spleen was similar to that in gastrointestinal tract, skin, heart, and brain and has moreover decreased over time.

In summary, the role of nanomaterials in optical detection systems for PON described until now range from: support providing stable immobilization of fluorophore, protection towards dye degradation, leakage or photo bleaching, providing diffusional barriers to minimize potential interferences, improving probe pharmacokinetics, as carriers for intracellular and targeted delivery, etc. up to an active role in detection as source of excitation of reporter probe or even as actual reporter providing the optical signal for PON detection. Although for each targeted application one should carefully balance the pros and cons of each approach as explained in section 4.2 and illustrated by the examples given below, SPNs provide a good starting point for further optimizations.

Practical applications

The range of applications involving nanomaterial-based optical methods systems focused on PON detection encompass: (i) quantitative detection of PON in spiked serum [42, 44, 45]; (ii) colorimetric detection of PON-induced DNA damage and screening of antioxidants in buffers [49]); (iii) imaging PON in live cells and animals. Quite excitingly, some endeavors aimed to fulfill a dual purpose: e.g. theranostics nanoparticles in which the capability for providing imaging of PON and ROS is doubled by the facilitation of photodynamic therapy [29] or nanoreactors having a dual functionality: (1) providing a means to study redox or cell reactions occurring on the top of their surface and (2) monitoring PON that diffuse inside the dye-modified nanoporous matrix [23].

There are many examples of applications of nanomaterial-based optical methods deserving a more detailed description of the nanomaterial role in the improvement of quantitative detection or imaging of PON. Some of the most challenging endeavours and where the power of optical detection proved most rewarding regard real-time imaging of events centered on PON-release and the exploitation of the imaging capability

delivered by novel probes for biomedical applications. These include new probes with targeted delivery for screening drug-induced hepatotoxicity and repair [47]; visualization of arthritic areas in mice limbs and monitoring the therapy with anti-arthritis drug methothrexate [48], theranostic nanoparticles for visualization and treatment of rupture-prone atherosclerotic plaques [29] etc.

For example, an SPN-based nanoprobe was proposed as a new tool for drug hepatotoxicity screening based on the in vivo detection of ROS and RNS [47]. The probe reunites four components and makes use of two energy transfer mechanisms-CRET and FRET- to achieve real time detection of PON/ClO^- and H_2O_2, produced in mice liver within minutes of acetaminophen or isoniazid administration (Fig. 16). The nanoprobe include a chemiluminescent substrate, CPPO responding to H_2O_2, a fluorescent dye, IR775S, sensitive to PON/ClO^- and a NIR-fluorescent polymer PFODBT acting as both CRET acceptor and FRET donor, according to the mechanism depicted in Fig. 16. The fourth component of the nanoprobe is a PEG-grafted poly(styrene) copolymer conjugated to galactose, with the role of targeting hepatocytes. Without any external light excitation, upon generation of H_2O_2 in the liver, CPPO is oxidized and emits a chemiluminescence signal. CRET takes place between the oxidized CPPO and nearby fluorophores PFODBT and IR775S and luminescence from both compounds is detected. Furthermore, PON and ClO^- oxidize IR775S, abolishing FRET and leading to the recovery of the fluorescence of matrix polymer PFODBT at 678 nm.

Another interesting optical probe with high applicative potential in diagnosis and treatment of atherosclerosis consists in ROS-responsive theranostic nanoparticles (MacTNP),

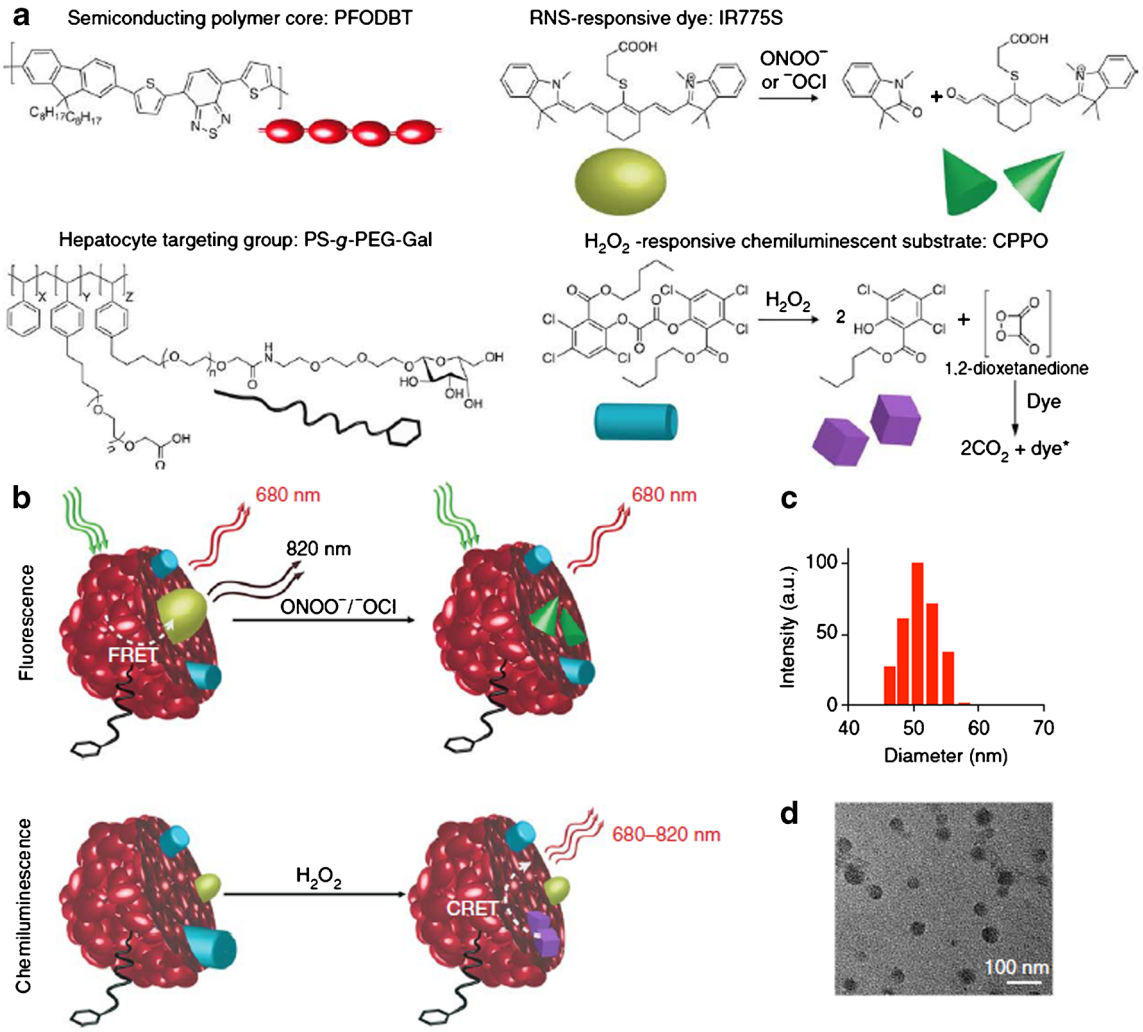

Fig. 16 **a** Design of CF-SPNs for detection of ROS and RNS, including four components: NIR fluorescent semiconducting polymer PFODBT (dark red), a PEG-grafted poly(styrene) copolymer conjugated to galactose (black), the H_2O_2-specific chemiluminescent substrate CPPO (light blue), and the ROS-sensitive dye IR775S (bright green) that is oxidised by ONOO− or ClO^- (dark green). **b** Schematic illustration of the mechanism for ONOO− or ClO^- and H_2O_2 detection with the CF-SPNs. **c** Distribution of the hydrodynamic diameter of CF-SPN as determined by dynamic light scattering. **d** Analysis of CF-SPN by transmission electron microscopy. Reproduced from [45] with permission from Nature Publishing Group

produced from a Chlorin e6 (Ce6)-hyaluronic acid (HA) conjugate for imaging and photodynamic therapy of activated macrophages (Fig. 17). Activated macrophages, which are considered a hallmark of unstable atherosclerotic plaques in the human body [29], generate ROS. The amphiphilic nanoparticles with a hydrodynamic size of 103.1 ± 38.4 nm include in their composition hyaluronic acid, which is known to be degraded by ROS, thus ensuring specific targeting of MacTNPs to activated macrophages. In the absence of ROS, in the extracellular environment MacTNPs are nonfluorescent due to self-quenching of the conjugated photosensitizer and display no phototoxicity. Under the action of PON generated inside LPS-activated macrophages in vitro, the particles are degraded, resulting in the release of Chlorin e6–HA fragments where the fluorescence of Chlorin e6 is recovered. Consequently, the photosensitizer emits bright near-infrared (NIR) fluorescence signals and generates singlet oxygen, making thus the nanoparticles highly phototoxic. The MacTNPs are believed to have a great potential in the selective imaging of activated macrophages and in subsequent photodynamic therapy of atherosclerosis with minimum side effects.

As shown by the applications detailed above and others in Table 2, there are many possibilities for optical imaging of PON with nanoprobes, all having advantages and limitations with regards to: (a) monitoring the dynamics of PON concentration (which requires reversible, fast responding probes), (b) high quality, ratiometric imaging of intracellular PON and of PON-producing events (e.g. activation of ROS production in macrophages) or (c) visualizing the effects of PON (such as DNA damage). For example, many optical nanoprobes rely on irreversible chemical transformations induced by PON to ensure sensitivity and selectivity of detection, one preferred strategy being the fragmentation of hyaluronan by PON. While not suitable for imaging decreases in PON levels, several of such probes were very successfully applied for high quality, ratiometric imaging of intracellular PON.

Challenges in the detection of PON with nanomaterial-based probes

Compared to the detection of other analytes, PON poses specific challenges related to its very short lifetime (half-life <1 s at physiological pH) and possible interferences by other ROS. Moreover, in complex environments such as cell cultures or for in vivo measurements, the probes should be biocompatible and display no cytotoxicity. Thus both fast and selective PON probes are needed, eluding passivation and non-specific binding in biological media. Several studies were performed in buffer at alkaline pH (Table 2), in the aim to ensure slower decomposition of the PON added in the medium. However, the relevance of such studies for physiological conditions, and real biological media remains untested. While electrochemical methods provide appropriate sensitivity and temporal resolution for monitoring fast events such as ROS bursts, the irreversibility of most optical nanoprobes prevents similar applications to monitor PON fluxes. A major limitation is also the selectivity of PON optical nanoprobes and electrochemical sensors, as most methods also respond to other ROS (Tables 1 and 2). Approaches to improve selectivity in electrochemical detection of PON are centered on either "chemical resolution" (using the "unique" electrochemical signal of PON) or on "selective chemical sensitivity" [61]. This consists in maximizing the signal for PON while diminishing the

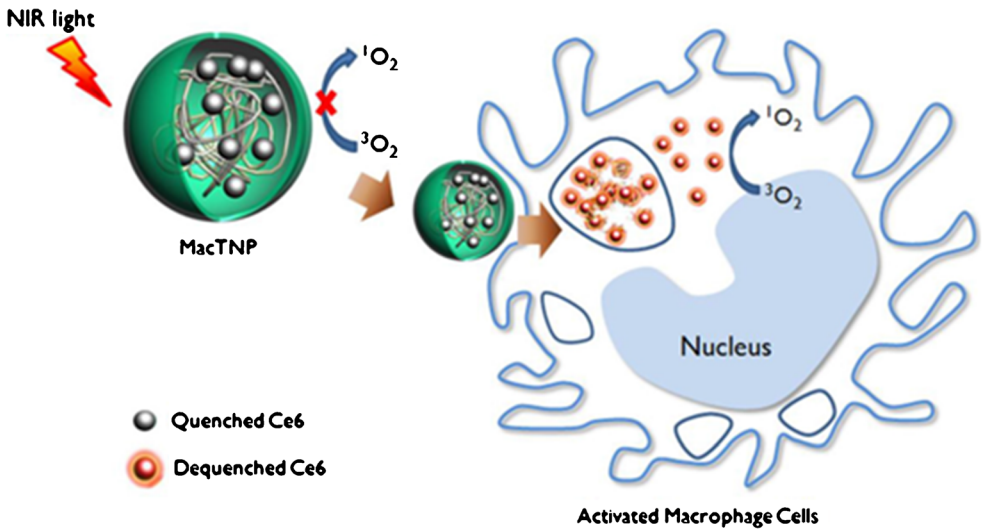

Fig. 17 Illustration of ROS-activatable theranostic nanoparticles MacTNP.for macrophage-targeted fluorescence imaging and photodynamic therapy. Degradation of MacTNP by ROS inside the activated macrophage triggers the fluorescence activation and singlet oxygen generation of Ce6s photosensitizers. Reproduced from [29] with permission under the terms of the Creative Commons License (http://creativecommons.org/licenses/by-nc-nd/3.0/)

overlapping signal from interfering species such as superoxide (O_2^-), nitric oxide (NO) or hydrogen peroxide (H_2O_2). These goals are accomplished with nanostructured electrodes and nanomaterials with new selectivity towards PON, electrode modification with catalytic films displaying high activity towards PON but negligible response towards interfering species and by use of permselective membranes to limit the access of interfering compounds to electrode surface. Adequate electrochemical techniques (e.g. Differential Pulse Amperometry, DPA) and tuned operating conditions to minimize disturbances by other species (e.g. at applied potentials close to 0 V), are sometimes combined with mathematical calculations, to extract the PON signal and differentiate it from that of the other interfering species in the medium [62]. Achievement of selectivity with optical nanoprobes relies on a combination between a PON-specific dye, nanoprobe design and the detection mechanism as discussed in section 4.4.3. However, as shown in Table 2, studies so far have investigated different ranges of interfering compounds, making direct comparison of methods' selectivity difficult. Some level of standardization of selectivity study will be welcomed in the field of PON research-for example by proposing a wide panel of possible interfering species to be consistently investigated. As the nanoprobes are shown not to be specific for PON, in many cases the identity of the signal attributed to PON is not clearly determined. To prove that the signal measured originates indeed from PON, proper controls should be included in the experiments, such as addition in the measurement medium of reagents known to prevent the formation of ROS or, on the contrary, to induce it. Typically used controls in the assessment of live macrophage cells include lipopolysaccharide (LPS), a stimulator of inducible nitric oxide synthase (iNOS) and phorbol 12-myristate 13-acetate (PMA), a stimulant for superoxide generation, to ensure generation of PON. To suppress PON-induced fluorescence effects in the macrophages, either a superoxide scavenger, e.g. 2,2,6,6-tetramethyl-1-piperidinyloxy (TEMPO) or an •NO synthase inhibitor, aminoguanidine (AG) is typically added to the macrophages. Besides bolus additions of chemically synthesized PON to the measurement media, additions of SIN-1 are used to mimic fluxes of PON generated in vitro and in vivo [26].

Risk assessment of nanomaterial-based probes needs to be performed on a case-by-case basis and little is yet known about the effect of the probes on the system that will be imaged –being this cells, tissues or whole animal.

Conclusions and perspectives

For the PON sensitive electrochemical methods, the use of reduced graphene oxide matrices or graphene modified with catalytic molecules towards peroxynitrite might be one way to go in the future for in vivo applications. Questions such as stability of the PON-sensitive matrix and cytotoxicity of such matrices are still not answered and certainly need further investigations. In addition, the efforts to develop individually addressable nano-electrode arrays are expected to increase in the near future.

Complementary to electrochemical tools, optical methods are particularly useful for providing images of high spatial resolution of PON-centered events. When choosing a detection method for PON one should consider first of all the desired scope: for example, while colorimetric methods and Au NPs with adsorbed DNA are used for screening antioxidants scavenging PON in vitro, nanocomposites with complex structures and up to 4 different components would be required for selective in vivo imaging of PON. There are significant challenges that still need to be overcome in PON optical detection. Reversibility of PON-controlled fluorescence of nanoprobes is mandatory for the real-time monitoring of dynamics of PON levels. However, the principle of the majority of optical probes developed so far involve irreversible transformations, including the otherwise appealing approach for ensuring selectivity for PON-induced activation of optical probes, by ROS-induced fragmentation of hyaluronan. Whereas new dyes with reversible, PON-specific fluorescence are actively researched, through combination with nanomaterials, as shown in this review, their sensitivity and selectivity can undoubtedly be further enhanced. However, the reversibility of all newly synthesized nanoprobes would need to be proven through multiple fluorescence "on-off" cycles. Notably, most of reports so far on optical nanoprobes for PON neglected the influence of pH and temperature on the acquired signal, although local pH variations or heating effects due to light exposure used for probe excitation are important. Together with a representative panel of interferents, including other ROS and metal ions, pH and temperature remain very important parameters to control in future studies to ensure the accuracy of PON assessment. Reproducibility has to be systematically investigated with several batches of nanoprobes, while data on probes' stability and cytotoxicity should be acquired in physiological-like conditions and for time periods typical for in vivo administration. Targeted delivery, appropriate blood circulation and clearance time from the body are additional challenges faced by optical probes; here, advances are expected to come from fast growing knowledge in the biomedical field featuring biocompatible nanomaterials and novel surface chemistries. Better, brighter and highly specific fluorescent probes, as well as application of new or so far underexplored optical methods can be envisaged in the future. Fluorescent dots of reduced graphene oxide having a lateral dimension of a few nm and spherical or elliptical shape have been developed and used for real-time molecular tracking in live cells [63] and various sensing applications [64], including the detection of H_2O_2 [65]. Upon adequate control and characterization [19], their applications for the detection of PON are just around the corner. Some optical methods used for

other ROS, such as Surface Enhanced Raman Scattering/ Spectroscopy (SERS) for example [66] have not yet been applied for PON detection but can be adapted to ensure selectivity for PON, e.g. by including PON selective compounds in nanocomposites of AgNPs-PEG-lipophilic dyes, with appropriate control of biocompatibility and reactivity.

Not in the least, exploration of photoacoustic (PA) probes using SPNs as NIR contrast agents [67] is a promising alternative with regards to PON imaging in vivo. The principle of PA probe is based on the generation of acoustic waves following the absorption of ultrashort light pulses, allowing imaging beyond the optical diffusion limit by integrating optical excitation with ultrasonic detection. This type of approach ensures highly specific molecular imaging with unprecedented performance, from millimeters to centimeters of tissue with resolutions in the 20–200 μm range and will undoubtedly be actively investigated in the future.

Acknowledgements Financial support by grants of the Executive Agency for Higher Education, Research, Development and Innovation Funding (UEFISCDI), Romanian Ministry of National Education and Scientific Research, project PN-II-PT-PCCA-2011-3.1-1809 (for AV) and PNII-ID- PCCE-2011–2-0075 (for MG) is gratefully acknowledged.

Compliance with ethical standards The author(s) declare that they have no competing interests.

References

1. Peteu SF, Boukherroub R, Szunerits S (2014) Nitro-oxidative species in vivo biosensing: challenges and advances with focus on peroxynitrite quantification. Biosens Bioelectron 58:359–373. doi:10.1016/j.bios.2014.02.025
2. Amatore C, Arbault S, Bouton C, Drapier J-C, Ghandour H, Koh ACW (2008) Real-time amperometric analysis of reactive oxygen and nitrogen species released by single Immunostimulated macrophages. Chembiochem 9(9):1472–1480. doi:10.1002/cbic.200700746
3. Beckman JS, Koppenol WH (1996) Nitric oxide, superoxide, and peroxynitrite: the good, the bad, and ugly. Am J Phys 271(5 Pt 1): C1424–C1437
4. Koppenol WH, Moreno JJ, Pryor WA, Ischiropoulos H, Beckman JS (1992) Peroxynitrite, a cloaked oxidant formed by nitric oxide and superoxide. Chem Res Toxicol 5(6):834–842. doi:10.1021/tx00030a017
5. Szabo C, Ischiropoulos H, Radi R (2007) Peroxynitrite: biochemistry, pathophysiology and development of therapeutics. Nat Rev Drug Discov 6(8):662–680. doi:10.1038/nrd2222
6. Pacher P, Beckman JS, Liaudet L (2007) Nitric oxide and peroxynitrite in health and disease. Physiol Rev 87(1):315–424. doi:10.1152/physrev.00029.2006
7. Amemiya S, Guo J, Xiong H, Gross DA (2006) Biological applications of scanning electrochemical microscopy: chemical imaging of single living cells and beyond. Anal Bioanal Chem 386(3):458–471. doi:10.1007/s00216-006-0510-6
8. Finkel T (2003) Oxidant signals and oxidative stress. Curr Opin Cell Biol 15(2):247–254. doi:10.1016/S0955-0674(03)00002-4
9. Halliwell B, Gutteridge JMC (1999) Free radicals in biology and medicine, 3rd edn. Oxford University Press, Oxford
10. Peteu SF, Banihani S, Gunesekera MM, Peiris P, Sicuia OA, Bayachou M (2011) Peroxynitrite and Nitroxidative Stress: Detection Probes and Micro-Sensors. A Case of a Nanostructured Catalytic Film. In: Oxidative Stress: Diagnostics, Prevention, and Therapy,. ACS Symposium Series, vol 1083. American Chemical Society, pp 311–339. doi:10.1021/bk-2011-1083.ch011
11. Oprea R, Peteu SF, Subramanian P, Qi W, Pichonat E, Happy H, Bayachou M, Boukherroub R, Szunerits S (2013) Peroxynitrite activity of hemin-functionalized reduced graphene oxide. Analyst 138(15):4345–4352. doi:10.1039/C3AN00678F
12. Koh WC, Son JI, Choe ES, Shim YB (2010) Electrochemical detection of peroxynitrite using a biosensor based on a conducting polymer-manganese ion complex. Anal Chem 82(24):10075–10082. doi:10.1021/ac102041u
13. Peteu S, Peiris P, Gebremichael E, Bayachou M (2010) Nanostructured poly(3,4-ethylenedioxythiophene)–metalloporphyrin films: improved catalytic detection of peroxynitrite. Biosens Bioelectron 25(8):1914–1921. doi:10.1016/j.bios.2010.01.008
14. Kubant R, Malinski C, Burewicz A, Malinski T (2006) Peroxynitrite/nitric oxide balance in ischemia/reperfusion injury-Nanomedical approach. Electroanalysis 18(4):410–416. doi:10.1002/elan.200503436
15. Uusitalo LM, Hempel N (2012) Recent advances in intracellular and in vivo ROS sensing: focus on nanoparticle and nanotube applications. Int J Mol Sci 13(9):10660. doi:10.3390/ijms130910660
16. Dowd A, Pissuwan D, Cortie MB Optical readout of the intracellular environment using nanoparticle transducers. Trends Biotechnol 32(11):571–577. doi:10.1016/j.tibtech.2014.09.004
17. Ruedas-Rama MJ, Walters JD, Orte A, Hall EAH (2012) Fluorescent nanoparticles for intracellular sensing: a review. Anal Chim Acta 751:1–23. doi:10.1016/j.aca.2012.09.025
18. Wolfbeis OS (2015) An overview of nanoparticles commonly used in fluorescent bioimaging. Chem Soc Rev 44(14):4743–4768. doi:10.1039/C4CS00392F
19. Merian J, Gravier J, Navarro F, Texier I (2012) Fluorescent nanoprobes dedicated to in vivo imaging: from preclinical validations to clinical translation. Molecules (Basel, Switzerland) 17(5): 5564–5591. doi:10.3390/molecules17055564
20. Jin R (2015) Atomically precise metal nanoclusters: stable sizes and optical properties. Nanoscale 7(5):1549–1565. doi:10.1039/C4NR05794E
21. Harkness KM, Cliffel DE, McLean JA (2010) Characterization of thiolate-protected gold nanoparticles by mass spectrometry. Analyst 135(5):868–874. doi:10.1039/b922291j
22. Zuo P, Lu X, Sun Z, Guo Y, He H (2016) A review on syntheses, properties, characterization and bioanalytical applications of fluorescent carbon dots. Microchim Acta 183(2):519–542. doi:10.1007/s00604-015-1705-3
23. Sciacca B, Pace S, Rivolo P, Geobaldo F (2012) Switching of fluorescence mediated by a peroxynitrite-glutathione redox reaction in a porous silicon nanoreactor. Phys Chem Chem Phys 14(15):5251–5254. doi:10.1039/C2CP23996E
24. Chen T, Hu Y, Cen Y, Chu X, Lu Y (2013) A dual-emission fluorescent nanocomplex of gold-cluster-decorated silica particles for live cell imaging of highly reactive oxygen species. J Am Chem Soc 135(31):11595–11602. doi:10.1021/ja4035939
25. Adegoke O, Nyokong T (2013) Probing the sensitive and selective luminescent detection of peroxynitrite using thiol-capped CdTe and

CdTe@ZnS quantum dots. J Lumin 134:448–455. doi:10.1016/j.jlumin.2012.08.002
26. Pu K, Shuhendler AJ, Rao J (2013) Semiconducting polymer nanoprobe for in vivo imaging of reactive oxygen and nitrogen species. Angew Chem Int Ed 52(39):10325–10329. doi:10.1002/anie.201303420
27. Lee H, Lee K, Kim I-K, Park TG (2009) Fluorescent gold nanoprobe sensitive to intracellular reactive oxygen species. Adv Funct Mater 19(12):1884–1890. doi:10.1002/adfm.200801838
28. Panizzi P, Nahrendorf M, Wildgruber M, Waterman P, Figueiredo J-L, Aikawa E, McCarthy J, Weissleder R, Hilderbrand SA (2009) Oxazine conjugated nanoparticle detects in vivo Hypochlorous acid and peroxynitrite generation. J Am Chem Soc 131(43):15739–15744. doi:10.1021/ja903922u
29. Kim HKY, Kim IH, Kim K, Choi Y (2014) ROS-responsive activatable photosensitizing agent for imaging and photodynamic therapy of activated macrophages. Theranostics 4(1):11. doi:10.7150/thno.7101
30. He X, Gao J, Gambhir SS, Cheng Z (2010) Near-infrared fluorescent nanoprobes for cancer molecular imaging: status and challenges. Trends Mol Med 16(12):574–583. doi:10.1016/j.molmed.2010.08.006
31. Kairdolf BA, Smith AM, Stokes TH, Wang MD, Young AN, Nie S (2013) Semiconductor quantum dots for bioimaging and Biodiagnostic applications. Annu Rev Anal Chem 6(1):143–162. doi:10.1146/annurev-anchem-060908-155136
32. Wang Y, Noël J-M, Velmurugan J, Nogala W, Mirkin MV, Lu C, Guille Collignon M, Lemaître F, Amatore C (2012) Nanoelectrodes for determination of reactive oxygen and nitrogen species inside murine macrophages. Proc Natl Acad Sci 109(29):11534–11539. doi:10.1073/pnas.1201552109
33. Peteu SF, Bose T, Bayachou M (2013) Polymerized hemin as an electrocatalytic platform for peroxynitrite's oxidation and detection. Anal Chim Acta 780:81–88. doi:10.1016/j.aca.2013.03.057
34. Peteu SF, Whitman BW, Galligan JJ, Swain GM (2016) Electrochemical detection of peroxynitrite using hemin-PEDOT functionalized boron-doped diamond microelectrode. Analyst 141(5):1796–1806. doi:10.1039/C5AN02587G
35. Hosu IS, Wang Q, Vasilescu A, Peteu SF, Raditoiu V, Railian S, Zaitsev V, Turcheniuk K, Wang Q, Li M, Boukherroub R, Szunerits S (2015) Cobalt phthalocyanine tetracarboxylic acid modified reduced graphene oxide: a sensitive matrix for the electrocatalytic detection of peroxynitrite and hydrogen peroxide. RSC Adv 5(2):1474–1484. doi:10.1039/C4RA09781E
36. Amatore C, Arbault S, Bruce D, de Oliveira P, Erard M, Vuillaume M (2000) Analysis of individual biochemical events based on artificial synapses using ultramicroelectrodes: cellular oxidative burst. Faraday Discuss 116:319–333 . doi:10.1039/B001448Fdiscussion 335-351
37. Filipovic MR, Koh AC, Arbault S, Niketic V, Debus A, Schleicher U, Bogdan C, Guille M, Lemaitre F, Amatore C, Ivanovic-Burmazovic I (2010) Striking inflammation from both sides: manganese(II) pentaazamacrocyclic SOD mimics act also as nitric oxide dismutases: a single-cell study. Angew Chem Int Ed Eng 49(25):4228–4232. doi:10.1002/anie.200905936
38. Amatore C, Arbault S, Bruce D, de Oliveira P, Erard LM, Vuillaume M (2001) Characterization of the electrochemical oxidation of peroxynitrite: relevance to oxidative stress bursts measured at the single cell level. Chemistry 7(19):4171–4179. doi:10.1002/1521-3765(20011001)7:19<4171::AID-CHEM4171>3.0.CO;2-5
39. Mason RP, Jacob RF, Corbalan JJ, Szczesny D, Matysiak K, Malinski T (2013) The favorable kinetics and balance of nebivolol-stimulated nitric oxide and peroxynitrite release in human endothelial cells. BMC Pharmacol Toxicol 14:48. doi:10.1186/2050-6511-14-48
40. Malinski T (2015) Using nanosensors for in situ monitoring and measurement of nitric oxide and peroxynitrite in a single cell. Methods Mol Biol 1208:139–155. doi:10.1007/978-1-4939-1441-8_11
41. Kaminska I, Das MR, Coffinier Y, Niedziolka-Jonsson J, Woisel P, Opallo M, Szunerits S, Boukherroub R (2012) Preparation of graphene/tetrathiafulvalene nanocomposite switchable surfaces. Chem Commun (Camb) 48(9):1221–1223. doi:10.1039/c1cc15215g
42. Simões EFC, da Silva JCGE, Leitão JMM (2014) Carbon dots from tryptophan doped glucose for peroxynitrite sensing. Anal Chim Acta 852:174–180. doi:10.1016/j.aca.2014.08.050
43. Gong Y, Yu B, Yang W, Zhang X (2016) Phosphorus, and nitrogen co-doped carbon dots as a fluorescent probe for real-time measurement of reactive oxygen and nitrogen species inside macrophages. Biosens Bioelectron 79:822–828. doi:10.1016/j.bios.2016.01.022
44. Simões EFC, Esteves da Silva JCG, Leitão JMM (2015) Peroxynitrite and nitric oxide fluorescence sensing by ethylenediamine doped carbon dots. Sens Actuat B-Chem 220:1043–1049. doi:10.1016/j.snb.2015.06.072
45. Simões EFC, Leitão JMM, da Silva JCGE (2016) Carbon dots prepared from citric acid and urea as fluorescent probes for hypochlorite and peroxynitrite. Microchim Acta 183(5):1769–1777. doi:10.1007/s00604-016-1807-6
46. Tian J, Chen H, Zhuo L, Xie Y, Li N, Tang B (2011) A highly selective, cell-permeable fluorescent nanoprobe for ratiometric detection and imaging of peroxynitrite in living cells. Chem Eur J 17(24):6626–6634. doi:10.1002/chem.201100148
47. Shuhendler AJ, Pu K, Cui L, Uetrecht JP, Rao J (2014) Real-time imaging of oxidative and nitrosative stress in the liver of live animals for drug-toxicity testing. Nat Biotechnol 32(4):373–380. doi:10.1038/nbt.2838
48. Chen Z, Liu Z, Li Z, Ju E, Gao N, Zhou L, Ren J, Qu X (2015) Upconversion nanoprobes for efficiently in vitro imaging reactive oxygen species and in vivo diagnosing rheumatoid arthritis. Biomaterials 39:15–22. doi:10.1016/j.biomaterials.2014.10.066
49. Chen L, Wu N, Sun B, Su H, Ai S (2013) Colorimetric detection of peroxynitrite-induced DNA damage using gold nanoparticles, and on the scavenging effects of antioxidants. Microchim Acta 180(7):573–580. doi:10.1007/s00604-013-0958-y
50. Jia X, Chen Q, Yang Y, Tang Y, Wang R, Xu Y, Zhu W, Qian X (2016) FRET-based Mito-specific fluorescent probe for ratiometric detection and imaging of endogenous peroxynitrite: dyad of Cy3 and Cy5. J Am Chem Soc 138(34):10778–10781. doi:10.1021/jacs.6b06398
51. Chen Z, Truong TM, Ai H-W (2016) CHAPTER 10 development of fluorescent probes for the detection of peroxynitrite. In: In: Peroxynitrite Detection in Biological Media: Challenges and Advances. The Royal Society of Chemistry, pp 186–207. doi:10.1039/9781782622352–00186
52. Li P, Han K (2016) CHAPTER 11 reversible near-infrared fluorescent probes for peroxynitrite monitoring. In: In: Peroxynitrite Detection in Biological Media: Challenges and Advances. The Royal Society of Chemistry, pp 208–226. doi:10.1039/9781782622352–00208
53. Zhang Q, Zhu Z, Zheng Y, Cheng J, Zhang N, Long Y-T, Zheng J, Qian X, Yang Y (2012) A Three-Channel fluorescent probe that distinguishes peroxynitrite from hypochlorite. J Am Chem Soc 134(45):18479–18482. doi:10.1021/ja305046u
54. Xu K, Chen H, Tian J, Ding B, Xie Y, Qiang M, Tang B (2011) A near-infrared reversible fluorescent probe for peroxynitrite and imaging of redox cycles in living cells. Chem Commun 47(33):9468–9470. doi:10.1039/C1CC12994E
55. Wang P, Zweier JL (1996) Measurement of nitric oxide and peroxynitrite generation in the postischemic heart. Evidence for

peroxynitrite-mediated reperfusion injury. J Biol Chem 271(46): 29223–29230. doi:10.1074/jbc.271.46.29223

56. Yasmin W, Strynadka KD, Schulz R (1997) Generation of peroxynitrite contributes to ischemia-reperfusion injury in isolated rat hearts. Cardiovasc Res 33(2):422–432. doi:10.1016/s0008-6363(96)00254-4
57. Fuchs B, Schiller J (2013) Glycosaminoglycan degradation by selected reactive oxygen species. Antioxid Redox Signal 21(7):1044–1062. doi:10.1089/ars.2013.5634
58. Kennett EC, Davies MJ (2007) Degradation of matrix glycosaminoglycans by peroxynitrite/peroxynitrous acid: evidence for a hydroxyl-radical-like mechanism. Free Radic Biol Med 42(8): 1278–1289. doi:10.1016/j.freeradbiomed.2007.01.030
59. Šoltés L, Mendichi R, Kogan G, Schiller J, Stankovská M, Arnhold J (2006) Degradative action of reactive oxygen species on hyaluronan. Biomacromolecules 7(3):659–668. doi:10.1021/bm050867v
60. Aillon KL, Xie Y, El-Gendy N, Berkland CJ, Forrest ML (2009) Effects of nanomaterial physicochemical properties on in vivo toxicity. Adv Drug Deliv Rev 61(6):457–466. doi:10.1016/j.addr.2009.03.010
61. Phillips PEM, Wightman RM (2003) Critical guidelines for validation of the selectivity of in-vivo chemical microsensors. TrAC Trends Anal Chem 22(8):509–514. doi:10.1016/S0165-9936(03)00907-5
62. Vasilescu A, Dinca V, Filipescu M, Rusen L, Hosu IS, Boukherroub R, Szunerits S, Dinescu M, Peteu SF (2016) CHAPTER 9 Recent Approaches to Enhance the Selectivity of Peroxynitrite Detection. In: In: Peroxynitrite Detection in Biological Media: Challenges and Advances. The Royal Society of Chemistry, pp 166–185. doi:10.1039/9781782622352–00166
63. Zheng XT, Than A, Ananthanaraya A, Kim D-H, Chen P (2013) Graphene quantum dots as universal fluorophores and their use in revealing regulated trafficking of insulin receptors in adipocytes. ACS Nano 7(7):6278–6286. doi:10.1021/nn4023137
64. Zheng XT, Ananthanarayanan A, Luo KQ, Chen P (2015) Glowing graphene quantum dots and carbon dots: properties, syntheses, and biological applications. Small 11(14):1620–1636. doi:10.1002/smll.201402648
65. Burmistrova N, Kolontaeva O, Duerkop A (2015) New nanomaterials and luminescent optical sensors for detection of hydrogen peroxide. Chemosensors 3(4):253. doi:10.3390/chemosensors3040253
66. Jiang C, Liu R, Han G, Zhang Z (2013) A chemically reactive Raman probe for ultrasensitively monitoring and imaging the in vivo generation of femtomolar oxidative species as induced by anti-tumor drugs in living cells. Chem Commun 49(59):6647–6649. doi:10.1039/C3CC43410A
67. Pu K, Shuhendler AJ, Jokerst JV, Mei J, Gambhir SS, Bao Z, Rao J (2014) Semiconducting polymer nanoparticles as photoacoustic molecular imaging probes in living mice. Nat Nanotechnol 9(3): 233–239. doi:10.1038/nnano.2013.302